Magnetic levitation as a suspension mechanism for cryogenic storage of hydrogen

Raymond Homan

Dissertation in partial fulfilment of the requirements for the degree Master of Engineering at the North-West University, Potchefstroom Campus

Supervisor: Professor Johan Markgraaff

December 2012

Acknowledgements

I would like to thank Professor Markgraaff for his guidance and contributions during this study. His knowledge and experience is of great value to any student. I also thank my parents, family and friends for their support and encouragement. I thank the North-West University for all resources allocated to me to make the completion of this study possible.

I also thank God the Father of our Lord Jesus Christ for His unfailing strength and love and for blessing me with the opportunity to further my studies as an engineer.

“For I am persuaded, that neither death, nor life, nor angels, nor principalities, nor powers, nor things present, nor things to come, nor height, nor depth, nor any other creature, shall be able to separate us from the love of God, which is in Christ Jesus our Lord.” Romans 8:38-39 King James Version Bible

Abstract

Current physical supports used in cryogenic storage vessels, in which liquid hydrogen is stored, conduct heat from the environment to the liquid hydrogen which causes the hydrogen temperature to rise and ultimately leads to hydrogen losses due to boil-off.

The focus of this study is to investigate magnetic levitation as a possible suspension mechanism, eliminating the use of current physical supports and so doing reducing hydrogen losses due to boil-off.

A conceptual design of a container which makes use of magnetic suspension is presented in this study. The concept is validated on the basis of the forces obtainable between a paramagnetic aluminium plate and an electromagnet, as well as the forces obtainable between a neodymium magnet and a bulk Yttrium-Barium-Copper-Oxide superconductor.

The forces between the paramagnetic aluminium plate and electromagnet were determined mathematically and tested experimentally. The forces between the magnet and superconductor were determined mathematically and by finite element modelling and simulations using ANSYS Multiphysics. The results obtained in the mathematical- and finite element studies were then validated experimentally.

It was found that the forces obtained experimentally between the aluminium plate and electromagnets are inadequate for magnetic suspension of the inner vessel given in the conceptual design. It was also found that the forces obtained experimentally and in the simulation studies for the magnet and superconductor of this study were inadequate due to shortcomings in the magnet and superconductor obtained for experimental tests.

The conclusion of this study is that electromagnetic levitation should not be used as a magnetic suspension mechanism for storage of liquid hydrogen. It is also concluded that superconducting levitation can not be used as a suspension mechanism for the concept presented in this study, unless the methods suggested to increase the levitation forces between the neodymium magnet and superconductor are executed.

Keywords: Cryogenics, Hydrogen storage, Magnetic suspension, Superconducting levitation.

Index

List of figures

List of tables

List of equations

Chapter 1: Introduction

Hydrogen may be an alternative fuel or energy carrier in the future as it is already undergoing research as a fuel source for use in fuel cells (Ramachandran & Menon, 1998). Hydrogen has to be combusted in oxygen to produce an exothermic reaction and release energy. In nature hydrogen exists in compounds with other elements only, but can be freed if hydrogen (H_2) is required for use. Hydrogen can be produced from any primary energy fuel like coal, oil and natural gas (Winter, 2009).

Hydrogen is used in numerous applications which include but is not limited to:

- *Petroleum processing*: Hydrogen is used to hydrogenate sulphur (S) and nitrogen (N) compounds to finally remove them as H_2S and NH_3 reducing NO_x and SO_x emissions in petroleum processing (Ramachandran & Menon, 1998).
- *Petrochemical production*: Hydrogen and carbon monoxide react over a catalyst at high pressures and temperatures to form methanol (Ramachandran & Menon, 1998).
- *Fertilizer production*: Ammonia, which is used in the production of fertilizer, is produced from hydrogen and nitrogen (N_2) (Ramachandran & Menon, 1998).

In the above mentioned applications and most areas where hydrogen is used, the need for proper storage of hydrogen arises. Metal hydrides are being researched as a possible storage medium (Sakintuna, *et al*., 2007). However, hydrogen is currently stored mainly in gas form which is either compressed (cH_2) or cryo-compressed (ccH_2) and liquid form ($L\text{-}H_2$). Cryo-compressed hydrogen is hydrogen gas stored at high pressure and sub-critical temperature for example at 38 MPa and 77 K (-196.15 °C).

Gaseous hydrogen is compressed and stored in cylinders. Filling times for these cylinders have been successfully tested between 40 seconds and 6 minutes (Mérida & Dicken, 2007). Although filling times of 40 seconds is possible, compressed hydrogen storage has disadvantages which include leakage of hydrogen from storage cylinders and low volumetric hydrogen storage density. Furthermore, the high mass and size of cylinders used for storage of compressed hydrogen contributes to transport difficulties.

The first of two major disadvantages for liquid hydrogen storage is the high energy cost to liquefy hydrogen. This is mainly due to the extremely low boiling point (approximately 20.3 K or -252.9 °C) and high heat capacity of hydrogen. The second of these is the constant loss of hydrogen during storage, because of heat transfer between the environment and the hydrogen stored, which causes hydrogen boil-off (van Vuuren, *et al*., 2009).

Figure 1 is a diagram which shows the operating range of cryogenic pressure vessels for hydrogen storage at temperatures ranging from 20 K (-253.15 °C) to 300 K (26.85 °C). This diagram also shows the density of the hydrogen due to the pressure at which it is stored and whether it is stored as a compressed gas or in liquid form.

For the diagram in Figure 1, the temperature scale is on the horizontal axis. Storage pressure is represented by the dotted lines and hydrogen density is presented on the left vertical axis. Solid lines represent the theoretical minimum work, which is the energy required to produce hydrogen in either the gaseous or liquid phase. The green shaded region represents the operating region of cryogenic pressure vessels for hydrogen storage (Aceves, *et al*., 2009).

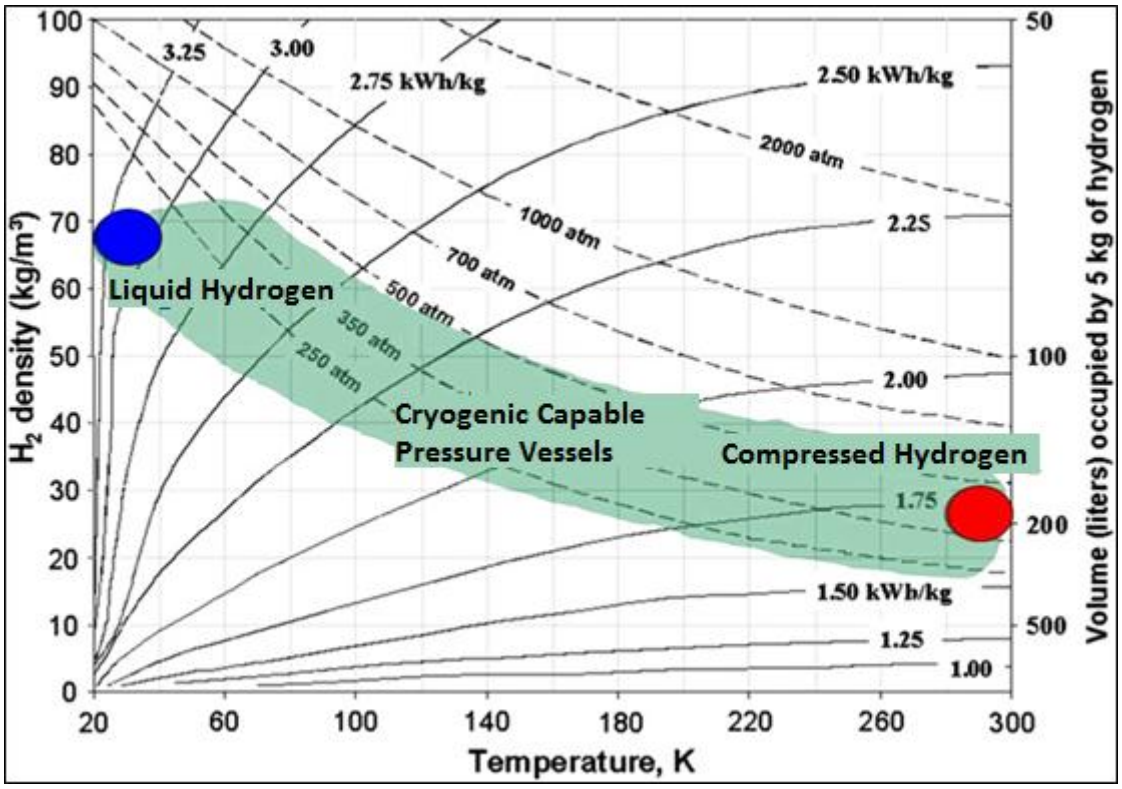

Figure 1: Diagram of hydrogen density at temperatures ranging from 20 K to 300 K for use in cryogenic capable pressure vessels (Modified after Aceves, *et al*., 2009).

The conditions required to store hydrogen as a compressed gas at ambient temperature are represented by the red dot in Figure 1. The volume occupied by 5 kg of compressed gaseous hydrogen at 300 K (26.85 °C) and approximately 400 atm is 200 l. Work of approximately 1.75 kWh/kg is required to produce cH_2 at these specific conditions.

The conditions required to store hydrogen as a liquid are represented by the blue dot in Figure 1. The volume occupied by 5 kg of L-H_2 at 20 K (-253.15 °C) and approximately 200

atm is 70 l. Work of approximately 3.25 kWh/kg is required to produce L-H_2 at these specific conditions.

Hand calculations were used to confirm the approximate values read from Figure 1. The storage volume required for 5 kg of cH_2 was calculated at approximately 213 l. The cH_2 has a relatively low density of 23.44 kg/m^3 compared to L-H_2 which is much more compact and has a higher density of approximately 71.26 kg/m^3.

The difference in density implies that approximately 70 l is required to store 5 kg L-H_2 compared to the 213 l required to store 5 kg cH_2 (Aceves, *et al*., 2009). A saving of 143 l in storage volume is achieved if 5 kg H_2 is stored in liquid form.

According to the USDOE (United States Department of Energy) hydrogen-powered vehicles should travel more than 300 miles (approximately 480 km) between fills to compete with petrol and diesel powered vehicles (Energy, 2011).

If hydrogen losses are ignored, calculations show that a car with an engine size of 118 kW requires approximately 14 kg hydrogen to travel 480 km. If L-H_2 is to be used, only 200 l storage volume is required compared to 600 l for cH_2, which is paramount for vehicular transport applications although this advantage comes with a cost penalty associated with the liquefaction energy requirement.

Different designs and patents for L-H_2 storage and transportation exist. Figure 2 is a schematic of a section view of US patent 4496073 which was filed for storage of cryogenic liquids (Silver & Dehaas, 1985).

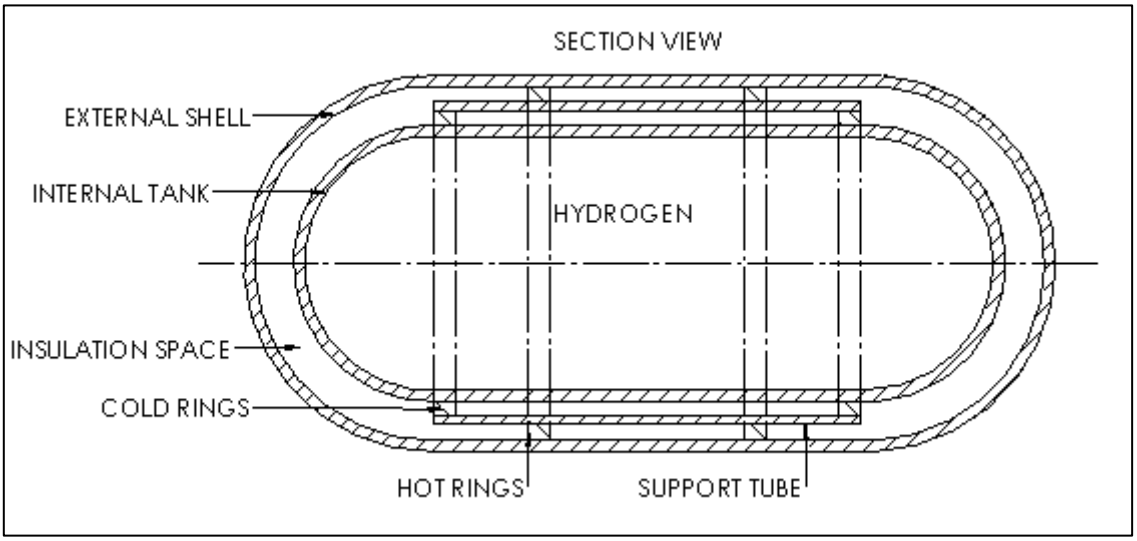

Figure 2: Schematic of a double wall cryogenic tank according to US patent 4496073 showing the use of hot and so-called cold rings for inner container suspension and insulation (Modified after Silver & Dehaas, 1985).

The container consists of an outer container, inner container, a support tube and support rings. By using the support tube and support rings the inner container is supported within the outer container minimizing conduction paths between the containers and environment. The empty space between the containers and the support tube is filled with proper insulation of which multilayer insulation is an example. The space between the two containers is then gas evacuated (Silver & Dehaas, 1985).

A schematic depiction of US patent 4680935 which was filed by Murai (1987) for the storage of cryogenic liquids is presented in Figure 3. The tank consists of an inner container suspended within an outer container by a single connecting pipe. The connecting pipe minimizes the heat transfer from the environment by limiting conduction to the neck of the pipe only.

Additionally, a vacuum is created in the space between the two containers to minimize convection from the outer container at ambient temperature and the inner container at cryogenic temperature. Any radiation effects are countered by shields placed between the containers (Murai, 1987).

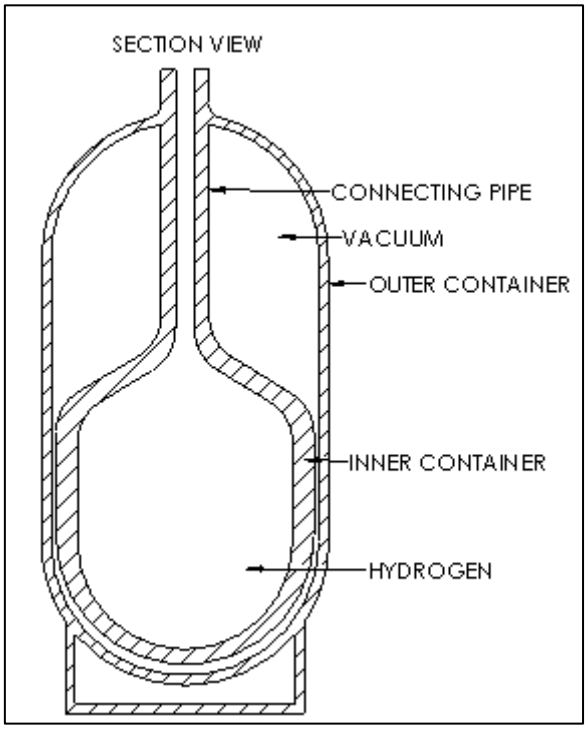

Figure 3: Schematic of a double wall cryogenic tank according to US patent 4680935 showing the use of a single connecting pipe for inner container suspension and insulation (Modified after Murai, 1987).

Presented in Figure 4, is a schematic depiction of a section view of US patent 6708502 filed for the storage of cryogenic fluids (Aceves, *et al*., 2004). This container consists of an inner

pressure vessel supported within an outer pressure vessel by means of insulated cross supports, to reduce heat transfer and reduce boil-off.

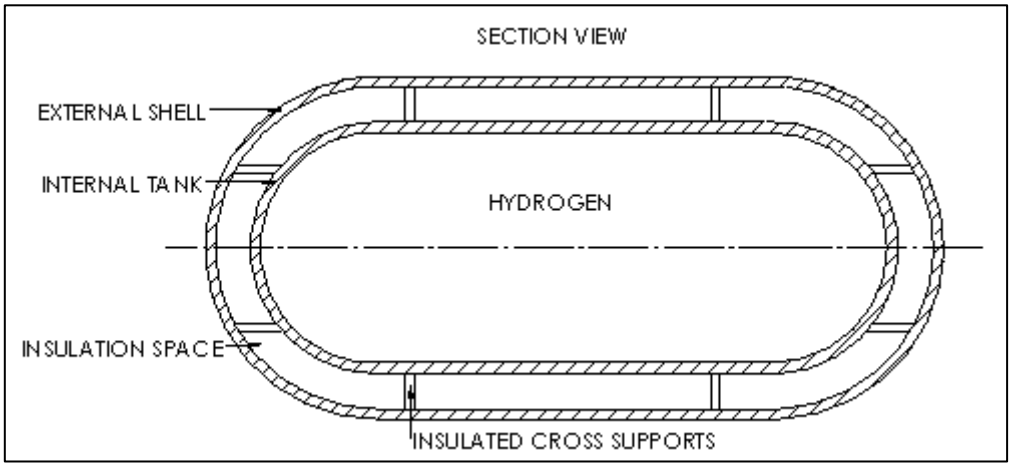

Figure 4: Schematic of a double wall cryogenic tank according to US patent 6708502 showing the use of insulated cross supports for inner container suspension and insulation (Modified after Aceves, *et al*., 2004).

Although the cryogen is stored in the inner container and thermal insulation is provided between the two containers in Figure 4, heat transfer still occurs from the environment to the inner container through these essential supports (Aceves, *et al*., 2004).

To further limit heat transfer through the required supports many cryogenic container designs make use of supports made from composites due to their low thermal conductivity at low temperatures (Reed & Golda, 1997). Composite supports include straps under tensile forces and struts under compressive forces. Figure 5 is a schematic presentation of a strap and different types of tubes.

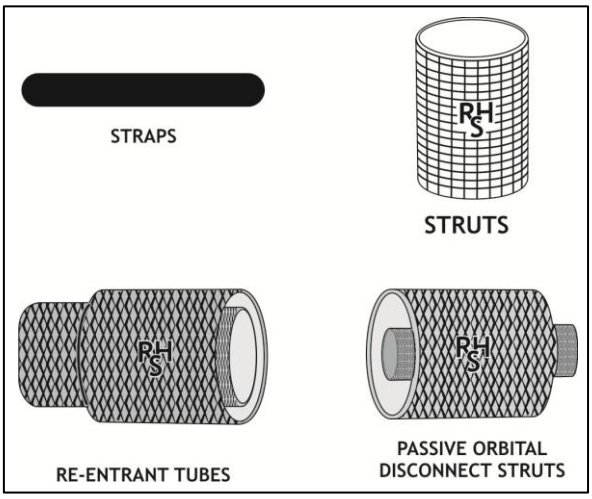

Figure 5: Schematic of cryogenic supports in which a strap and struts are illustrated (Modified after Reed & Golda, 1997).

An example of support struts that was mentioned earlier is the cross supports of US patent 6708502 in Figure 4. These support types are fibre reinforced and traditionally epoxy-based composites (Reed & Golda, 1997).

For cryogenic containers that use straps as supports, between six and eight straps are used to balance the applied forces that are found between the warm and cold structures of the cryogenic containers. To combat thermal influences between these structures, support straps are made as long and thin as possible to maximise the thermal path (Reed & Golda, 1997).

Alumina and glass fibres (such as E- and S-glass) are examples of the different fibres used to reinforce straps. As mentioned earlier straps may be epoxy-based or reinforced with PEEK (polyetheretherketone), a type of resin matrix (Reed & Golda, 1997).

For a container setup in which L-H_2 (20 K or -253.15 °C) is stored of which one container is kept within another such as in Figure 2 and Figure 4 the temperature gradient between the outer container (ambient temperature 300 K or 26.85 °C) and the inner container is 280 K. Due to the fact that heat flows from warmer regions to colder regions, a temperature rise for the cryogen takes place due to the addition of heat through the supports mentioned. This rise in temperature in turn causes boil-off of the L-H_2.

Calculations of heat transfer and the effects thereof were carried out for a double wall cryogenic container for which an inner container is suspended within an outer container with the use of carbon fibre straps. Conductivity values for carbon fibre supports given by Reed and Golda (1997) were used for this calculation.

Heat transfer through one carbon strap was calculated at 7.2 mW which results in a calculated hydrogen loss of approximately of 1.4 g/day due to boil-off. For six straps the total heat transfer through the straps is 43.2 mW, resulting in hydrogen boil-off of 8.4 g/day. The calculations and results for heat transfer through carbon straps are discussed in Appendix A.

Tubes (also called struts) are also used as supports in cryogenic containers. Tubes are built to have minimal thickness and are usually hollow cylinders to minimize the heat transfer area, reducing heat transfer to the cryogen in the container (Reed & Golda, 1997).

Calculations for the heat transfer through E-glass support tubes were conducted for a design similar to that in Figure 4 in which a double wall cryogenic container makes use of E-glass tubes to suspend an inner container within an outer container.

One tube has a calculated heat transfer of approximately 5.7 mW, which corresponds to a hydrogen loss of approximately 1.1 g/day due to boil-off. For six struts, the heat transfer was calculated at approximately 34 mW which results in a hydrogen loss of approximately 6.6 g/day due to boil-off. The calculations and results for heat transfer through E-glass tubes are discussed in Appendix A.

Van Vuuren, *et al.* (2009) suggested a concept (depicted in Figure 6) for the cryogenic storage of hydrogen in vehicles and other transport systems that may adhere to the USDOE requirements. In Figure 6, the inner container, which contains ccH_2, is contained within an outer container. Van Vuuren, *et al.* (2009) proposed to use titanium wires (instead of other structured material supports) to support the inner container within the outer container to minimize conduction to the inner container.

The suggested cross sectional area of a wire to achieve a heat transfer of maximum 0.5 W is 3.56 mm^2. If six wires are used to stabilize the inner container in the different axes and the effects of MLVSI and the nitrogen are ignored, the heat transfer to the hydrogen container is 3 W (van Vuuren, *et al*., 2009).

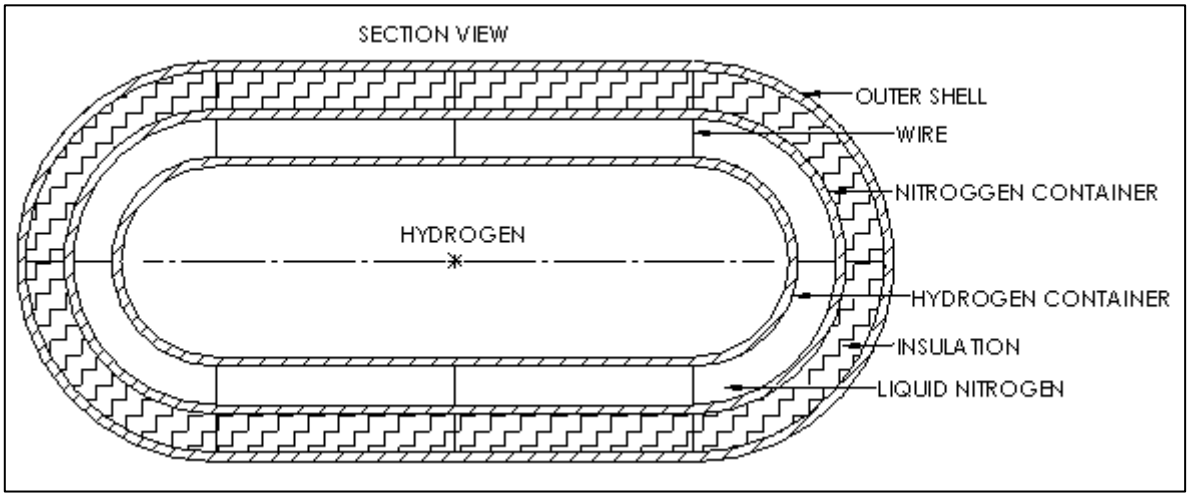

Figure 6: Schematic of a double wall cryogenic tank showing the use of titanium wires as supports for inner container suspension and insulation (Modified after van Vuuren, *et al*., 2009).

To further minimize heat flow to the inner vessel, Van Vuuren, *et al.* (2009) proposed to thermally insulate the outer vessel with MLVSI (multi-layer vacuum super insulation) and by filling the outer container with $L\text{-}N_2$ (liquid nitrogen). The $L\text{-}N_2$ absorbs heat that is conducted from the environment through the vessel walls and wire supports which would otherwise be absorbed by the hydrogen. The $L\text{-}N_2$ is then boiled-off and due to the cooling effect of evaporation, the hydrogen in the inner vessel is kept at 77 K (-196.15 °C).

Van Vuuren, *et al.* (2009) states that the heat flowing into the container, by means of conduction through the wire supports, insulation and pipe neck can be limited to 2.5 W. For this 2.5 W, a liquid nitrogen bleed-off rate of approximately 1 kg/day is required to keep the hydrogen from increasing in pressure and temperature and ultimately having to be bled off (van Vuuren, *et al*., 2009).

Once all the nitrogen has evaporated, the temperature of the hydrogen container will start to rise which in turn causes a pressure increase in the hydrogen container. To then counter the increase in pressure and keep the container at a safe operating pressure, hydrogen must be bled-off. The initial hydrogen bleed-off rate is 160 g/day. This initial bleed rate will increase with an increase in the hydrogen container's temperature. The hydrogen temperature will increase by 3.1 °C/day (van Vuuren, *et al*., 2009).

The advantage of this design is that a four day window exists wherein nitrogen can be refilled before completely being evaporated, thus before the hydrogen is required to be bled off. Compared to the container that makes use of struts (container using struts had less calculated hydrogen losses than container using straps) the concept of Van Vuuren, *et al.* (2009) will have 0 % hydrogen loss for the first four days, whereas the container using struts will have lost 26.4 g H_2 by the fourth day.

Although the concept suggested by Van Vuuren, *et al.* (2009) has the advantage of nitrogen as thermal insulation which ensures a longer storage period without hydrogen loss, there is a cost penalty due to the infrastructure required for nitrogen storage at hydrogen filling stations.

In summary, methods which are used to reduce conduction of heat from the environment to the cryogen include the use of nitrogen as a thermal insulator, drawing a vacuum between the containers (van Vuuren, *et al*., 2009), physical supports such as support rings (Silver & Dehaas, 1985), carbon and other fibre reinforced straps, E-glass tubes (Reed & Golda, 1997), titanium wires (van Vuuren, *et al*., 2009), insulated cross supports (Aceves, *et al*., 2004) and thin connecting pipes (Murai, 1987).

Although all these schemes lower the thermal conduction from the outer container to the inner container, there is still some level of conduction from the environment to the cryogen through the above mentioned support methods that contributes to hydrogen losses due to boil-off.

1.1 Problem statement

Heat from the environment is added to the cryogenic fluid in cryogenic containers, by means of conduction through current support systems implemented in cryogenic containers. This heat addition contributes to a temperature rise of the cryogen and ultimately leads to boil-off resulting in unwanted losses of the fluid.

1.2 Aim

A possible method to further reduce the contribution of current support systems to hydrogen boil-off is the use of magnetic suspension of the inner containers while eliminating any other form of physical support. The aim of this study therefore, is to investigate the feasibility of magnetic suspension for cryogenic containers.

Chapter 2: Literature Study

2.1 Background

2.1.1 Magnetism

All materials respond to magnetic fields, and it is suggested that there is no such thing as a "nonmagnetic" material. However the response to magnetic fields is not the same for all materials which leads to the conclusion that some materials are strongly magnetic while others are weakly magnetic. Weak magnetic materials are usually referred to as "nonmagnetic" materials (Askeland & Phulé, 2003).

The relationship between magnetic field, magnetization and permeability is explained using a current passing through a wound coil as shown in Figure 7. A magnetic field is produced when the electric current passes through the coil.

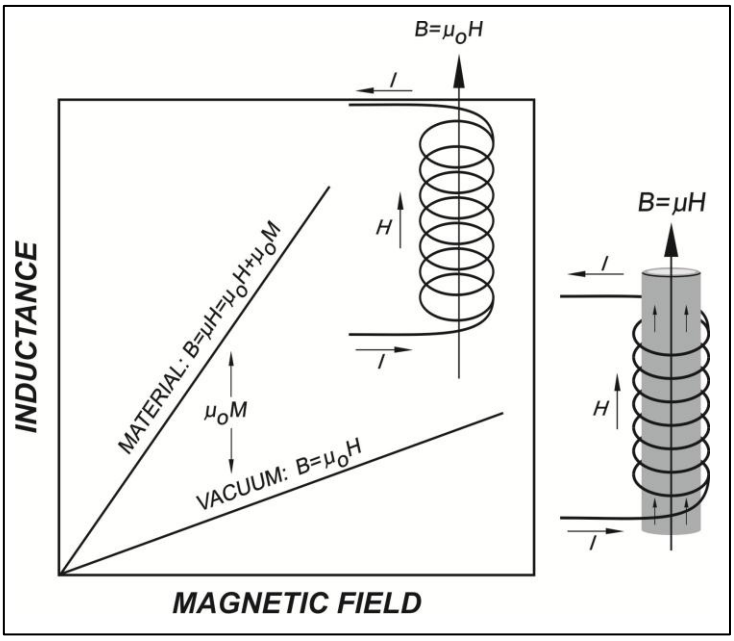

Figure 7: Schematic illustration of the difference in inductance induced by electromagnets of an electromagnet with a core and an electromagnet without a core in a vacuum or air (Modified after Askeland & Phulé, 2003).

The magnetic field strength ***H***, measured in A/m, is then given by

$$\boldsymbol{H} = \frac{n\boldsymbol{I}}{l} \qquad \textbf{(1)}$$

where *n* is the number of turns, ***I*** is the current (A) and *L* is the length of the coil (m).

When the magnetic ***H***-field is applied in a vacuum, magnetic flux lines are induced. The number of flux lines called magnetic flux density or inductance is related to the ***H***-field by

$$\boldsymbol{B} = \mu_0 \boldsymbol{H} \quad \textbf{(2)}$$

where ***B*** is the magnetic flux density or inductance measured in Tesla and μ_0 is the permeability constant for free space (in vacuum) 4π x 10^{-7} Henry/m (Askeland & Phulé, 2003).

When placing a material core in the magnetic field, the magnetic flux density is determined by the interaction of the induced and permanent magnetic dipoles with the field. The flux density is now given by

$$\boldsymbol{B} = \mu \boldsymbol{H} \quad \textbf{(3)}$$

where μ is the permeability of the material in the field (Askeland & Phulé, 2003).

A greater number of flux lines which do more work are generated if the magnetic moments reinforce the applied field. That is, if $\mu > \mu_0$ there is a magnification of the magnetic field. If $\mu < \mu_0$, the magnetic moments oppose the field.

The relationship of μ to μ_0 is called the relative permeability (μ_r). For a large relative permeability the magnetic field is amplified by the material (Askeland & Phulé, 2003). This relationship is given by

$$\mu_r = \frac{\mu}{\mu_0} \quad \textbf{(4)}$$

The ***H***-field causes magnetization (***M***) of the core material which partially contributes to the total flux density ***B***. The equation for magnetic flux density is then rewritten as

$$\boldsymbol{B} = \mu_0 \boldsymbol{H} + \mu_0 \boldsymbol{M} \quad \textbf{(5)}$$

where $\mu_0\boldsymbol{H}$ is the component of inductance caused by the applied field (***H***-field) and $\mu_0\boldsymbol{M}$ is the component of inductance caused by the magnetic core material.

According to Askeland and Phulé (2003) the amplification produced by a material is given by the relationship of magnetization to the applied field. This relationship is called the magnetic susceptibility and is given by

$$\chi_m = \frac{\boldsymbol{M}}{\boldsymbol{H}} \quad \textbf{(6)}$$

As with μ_r, χ_m also refers to the degree to which a material enhances the magnetic field (Askeland & Phulé, 2003). The relationship between μ_r and χ_m is given by

$$\mu_r = 1 + \chi_m \quad \textbf{(7)}$$

Different materials which differ in μ_r magnitude exhibit different magnetic behaviour. Paramagnetic behaviour, ferromagnetic behaviour and diamagnetic behaviour are reviewed in the following paragraphs.

Materials which have unpaired electrons have a net magnetic moment associated with each atom due to electron spin. An applied magnetic field causes the dipoles to line up with the field inducing a positive magnetization. There is no interaction between the dipoles and therefore large forces are required to align all the dipoles. As soon as the magnetic field is removed in these materials called paramagnetic materials, this effect is lost. (Askeland & Phulé, 2003).

Paramagnetic materials have $\mu > \mu_0$, and therefore they also have low μ_r values and low positive χ_m values. The magnitude for χ_m of paramagnetic materials ranges from 10^{-4} to 10^{-5}. Paramagnetic materials include aluminium, titanium and alloys of copper (Askeland & Phulé, 2003).

Ferromagnetism is caused by the unfilled energy levels in the 3*d* level of iron, nickel and cobalt. The permanent unpaired dipoles, effortlessly line up with the imposed magnetic field due to the mutual reinforcement of the dipoles. Due to ferromagnetic materials having $\mu >> \mu_0$, they also have high μ_r values and high positive χ_m values, and therefore ferromagnetic materials are strong magnetic materials (Askeland & Phulé, 2003).

Large magnetizations are obtained even for small magnetic fields which deliver magnetic susceptibilities of the order 10^6 (Askeland & Phulé, 2003). Rare earth magnets are ferromagnetic and contain rare earth metals such as neodymium which is used for neodymium (NdFeB) magnets. NdFeB magnets are often used for magnetic levitation purposes in combination with superconductors.

Diamagnetic materials repel applied fields. When a magnetic field acts on an atom a magnetic dipole is induced by the field over the atom. This field influences the magnetic moment caused by the orbiting electrons. The magnetic field is then opposed by the dipoles which cause the magnetization to be less than zero (Askeland & Phulé, 2003).

Diamagnetism gives a relative permeability of about 0.99995 which results in a negative susceptibility (-0.00005). Diamagnetic materials have $\mu < \mu_0$, causing them to have low μ_r values and low negative χ_m values. Copper, silver and gold are diamagnetic at room temperature. Of importance however, is that superconductors display pure diamagnetic behaviour ($\chi_m = -1, \mu_r = 0$) below their critical temperatures (Askeland & Phulé, 2003).

2.1.2 Superconductivity

Heike Kamerlingh Onnes discovered superconductors when he discovered superconductivity in metals at very low temperatures (De Bruyn Ouboter, 1997). Research has shown that some materials become superconducting at low temperatures such as lead at 7.2 K (-265.95 °C), niobium at 8 K (-265.15 °C), niobium nitride at 15 K (-258.15 °C) and niobium germanium at 23 K (-250.15 °C) (Jha, 1988). Such superconductors are referred to as low temperature superconductors (LTSC).

High temperature superconductors (HTSC) are superconductors which become superconducting at higher temperatures compared to LTSC that become superconducting at extremely low temperatures.

Paul Chu discovered yttrium barium copper oxide ($Y_1Ba_2Cu_3O_{x-7}$ or YBCO) an HTSC compound which has a transition temperature of 90 K (-183.15 °C) (Jha, 1988). Other HTSC materials also exist of which most are compounds of yttrium, bismuth or thallium such as BiSrCaCuO that becomes superconducting at 110 K (-163.15 °C) and TlBaCaCuO at 125 K (-148.15 °C) (Jha, 1988).

Superconductivity has two very impressive and important properties. The first property is that once a material is cooled below its T_c (superconducting transition temperature) it loses all its resistivity making a transition from finite resistivity ρ to $\rho = 0$. In other words it conducts direct current without resistance thus it's conductivity becomes infinite ($\sigma = \infty$) (Fossheim & Sudboe, 2004; Iwasa, 2009).

The second property is the change in magnetic susceptibility (χ) where above T_c the value for χ is a small positive value, which causes the material to be paramagnetic, but below T_c it becomes $\chi = -1$, thus it is a perfect diamagnet (Askeland & Phulé, 2003; Fossheim & Sudboe, 2004; Iwasa, 2009).

Meissner and Ochsenfeld discovered perfect diamagnetism ($\mu_r = 0$) for a superconductor in the superconducting state and observed that an applied magnetic field penetrates the superconductor above its T_c (Fossheim & Sudboe, 2004).

However, as soon as the temperature drops below T_c the field is expelled from the superconductor (Bleuler, *et al*., 2009; Fossheim & Sudboe, 2004). This means that the flux density inside the superconductor becomes zero ($\boldsymbol{B} = 0$) below T_c. This expelling of the magnetic field from the superconductor is known as the Meissner effect.

Figure 8 presents the change in resistivity and susceptibility when the Meissner effect is induced in a superconductor as the temperature changes from $T > T_c$ to $T < T_c$ (Fossheim & Sudboe, 2004).

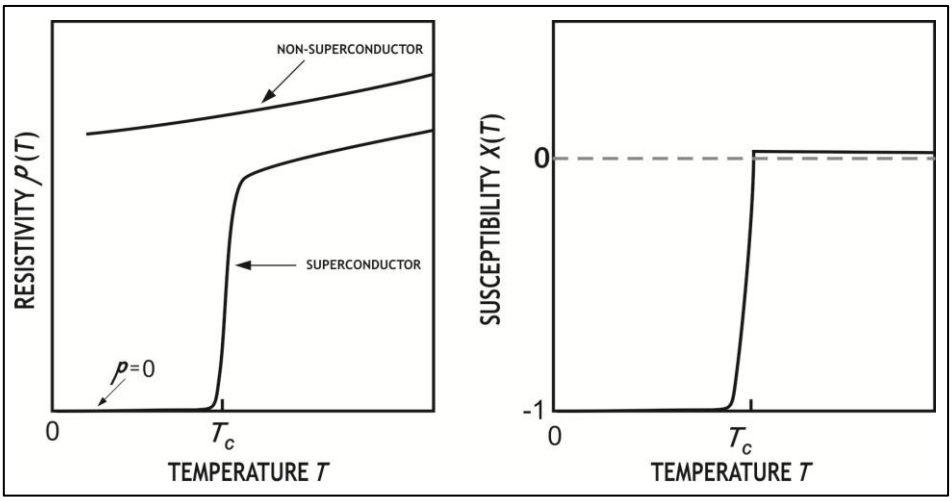

Figure 8: Two schematics which illustrate the basic characteristics of superconductors. The effects on resistivity (left) and susceptibility (right) for superconductors are given as functions of temperature (Modified after Fossheim & Sudboe, 2004).

For a magnetic body in the superconducting state, the magnetic flux density (Equation 5) is set equal to zero, which results in

$$\boldsymbol{B} = \mu_0 \boldsymbol{H} + \mu_0 \boldsymbol{M} = 0 \qquad \textbf{(8)}$$

which in a superconductor gives,

$$\boldsymbol{M} = -\boldsymbol{H}. \qquad \textbf{(9)}$$

The substitution of Equation 9 into Equation 6 then gives a magnetic susceptibility of -1 as presented by

$$\chi = \frac{d\boldsymbol{M}}{d\boldsymbol{H}} = -1 \qquad \textbf{(10)}$$

Substituting Equation 10 into Equation 7 results in a zero relative permeability,

$$\mu_r = 1 + \chi = 0 \qquad \textbf{(11)}$$

Both $\mu_r = 0$ and $\chi = -1$ are used to describe the Meissner effect (Fossheim & Sudboe, 2004).

When the superconductor's temperature drops below T_c, shielding currents arise in the superconductor surface and a field both inside and outside the superconductor is created. The applied ***H***-field and induced fields then cancel out exactly inside the superconductor, while the fields on the outside add, giving rise to expulsion of the ***B***-field from the superconductor (Fossheim & Sudboe, 2004).

Therefore there is zero ***B***-field in the superconductor and an increased field exists on the outside near the superconductor as depicted in Figure 9 (Fossheim & Sudboe, 2004). The Faraday lines (flux lines) in the normal state pass through the superconductor with no hindrance, but for the superconductor in the superconducting state all lines are forced to pass on the outer side of the superconductor (Fossheim & Sudboe, 2004).

As depicted in Figure 9, the flux lines are densest at the equator in the superconducting state. The flux lines are also less dense around the poles in the superconducting state than in the normal state (Fossheim & Sudboe, 2004).

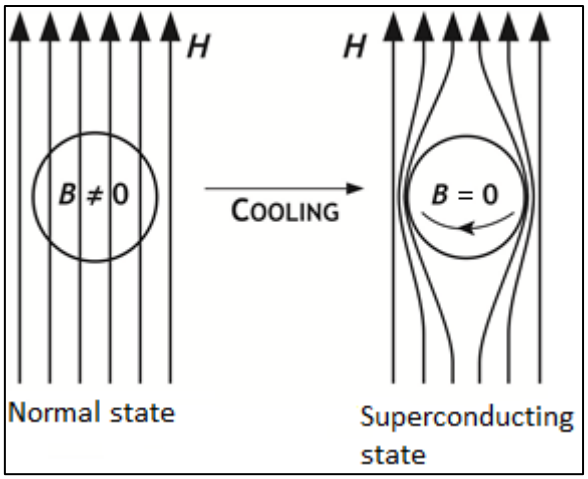

Figure 9: Schematic illustrating the field lines passing through a superconductor in the normal state and field lines being expelled by the superconductor in the superconducting state (Modified after Fossheim & Sudboe, 2004).

Superconductors in the superconducting state are used for superconducting levitation. An example of superconducting levitation is when a magnet levitates above a superconductor due to the forces generated by the interaction between the magnet and superconductor as mentioned in Chapter 2.1.1. In Chapter 2.1.3 the fundamentals of superconducting levitation is discussed.

2.1.3 Superconducting levitation fundamentals

As discussed in Chapter 2.1.2, a superconductor excludes field lines from itself when in the Meissner state. However it is important for magnetic flux to penetrate the superconductor in the form of discrete flux lines to achieve stable superconducting levitation (Chen, *et al*., 1998; Fuchs, *et al*., 2005).

In an experiment by Fuchs *et al.* (2005) a superconductor was cooled from $T > T_c$ to $T < T_c$ in the presence of a magnetic field. The flux lines created paths for the magnetic flux within

the superconductor. This caused the field lines to be pinned in the superconductor and not excluded as previously discussed for the Meissner effect. Cooling of the superconductor from $T > T_c$ to $T < T_c$ within a magnetic field is called field cooling (Fuchs, *et al*., 2005).

In an experiment by Chen *et al.* (2007) a magnet was brought close enough to a superconductor, after being zero-field cooled. The flux was forced through the superconductor by the magnet and trapped in the superconductor causing the magnet to levitate above the superconductor (Chen, *et al*., 2007).

Zero-field cooling is when the superconductor is cooled in the absence of a magnetic field. Shielding currents are induced in the outer surface of the superconductor while the superconductor undergoes zero-field cooling thus demonstrating the Meissner effect (Chen, *et al*., 1998).

Experiments performed by Fuchs *et al.* (2005) and Chen *et al.* (2007) demonstrated flux trapping which is the pinning of the magnetic field in the superconductor. Fuchs *et al.* (2005) proved that field lines could be pinned while field cooling the superconductor.

Chen *et al.* (2007) proved that a magnetic field could be pinned after the superconductor had been zero-field cooled. Field cooling is advantageous above zero-field cooling because inhomogeneous field distribution is frozen within the superconductor due to flux pinning (Fuchs, *et al*., 2005).

In summary a superconductor is a material that conducts current without loss and expels magnetic fields due to the Meissner effect ($\mu_r = 0$) (Fossheim & Sudboe, 2004). However a superconductor in the superconducting state may pin a magnetic field within itself if it is field-cooled (Fuchs, *et al*., 2005). A field may also be forced into the superconductor after being zero-field cooled (Chen, *et al*., 2007). Both examples of field pinning result in magnetic levitation. For this reason, superconductors are used for magnetic suspension purposes as discussed next in Chapter 2.1.4.

2.1.4 Magnetic suspension

Magnetic suspension is the suspension of an object with the use of a magnetic field. Examples of magnetic suspension include an electromagnet that makes use of fields induced by alternating current to levitate above an aluminium plate and a magnet that levitates above a superconductor which is the result of diamagnetism, more specifically superconductivity.

Lewin (2002) showed how magnetic levitation may be achieved using an electromagnet and a paramagnetic metal plate. An alternating current flowing in a coil induces a magnetic field,

as shown in Figure 10. The right hand rule shows that the magnetic field produced by the coil is downward.

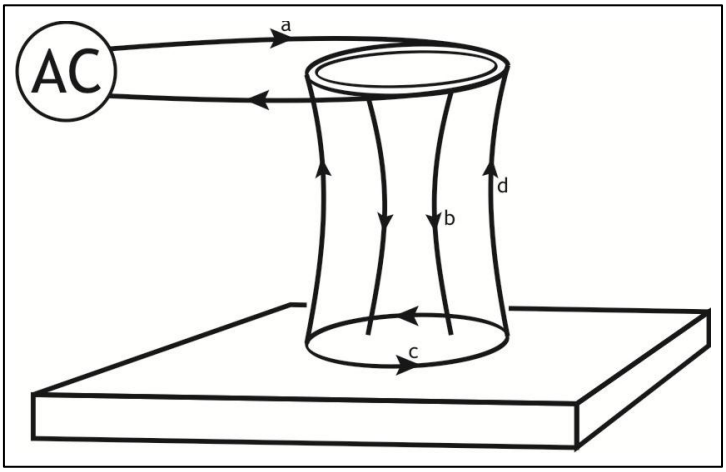

Figure 10: Schematic of an electromagnet inducing an eddy current in a paramagnetic plate causing magnetic levitation of the electromagnet above the plate.

The magnetic field of the electromagnet induces eddy currents, presented in Figure 10, in the nearby paramagnetic plate which flow in the opposite direction to the current in the coil. The eddy current then induces a magnetic field that works in the opposite direction as the field of the electromagnet, as shown in Figure 10.

These magnetic fields oppose each other causing the electromagnet and the aluminium plate to repel one another like two bar magnets with their north poles against each other. The magnet then freely moves above the plate due to the opposition of the two fields achieving magnetic levitation.

The magnetic force (***F***) produced by an electromagnet is given by

$$\boldsymbol{F} = \frac{(N\boldsymbol{I})^2 \mu_0 A}{(2g^2)} \qquad \textbf{(12)}$$

where *N* is the number of wire windings, ***I*** is the current (Ampere) flowing through the windings, *A* is the cross sectional area (m^2) of the core material which is typically a paramagnetic material (a material which keeps minimal or none of its magnetization once current is switched off), *g* is the air gap (distance) between the electromagnet and the surface of the plate, measured in meters (Clarke, R., 2011).

Lewin (2002) claims that a magnet (for example NdFeB) exerts pressure on a superconductor in the superconducting state. This pressure is caused by the force of the magnet which acts on the superconductor when the field lines are repelled by the superconducting sample. This pressure is given by,

$$P = \frac{\boldsymbol{B}^2}{2\mu_0} \quad \textbf{(13)}$$

where *P* is the pressure measured in Pascal (Lewin, 2002).

To determine the levitation force delivered by a permanent magnet on a superconductor in the Meissner state, which causes the magnet to levitate above the superconductor, Equation 13 is multiplied by the cross sectional area of the magnet which gives

$$\boldsymbol{F} = \frac{\boldsymbol{B}^2 A}{2\mu_0} \quad \textbf{(14)}$$

where ***F*** is the force (N), *A* is the area (m^2) of the magnet. This levitation force between the superconductor and the magnet is the result of the interaction between the magnetic field of a ferromagnetic material and a diamagnetic material (Lewin, 2002).

Superconducting levitation by means of forces generated between magnets and subcritical cooled superconductors in the Meissner state is also an example of magnetic suspension which is used in passive magnetic bearings.

Magnetic bearings are categorised as active magnetic bearings or passive magnetic bearings. Active magnetic bearings (AMBs) make use of electromagnets while passive magnetic bearings (PMBs) make use of permanent magnets (which are made from ferromagnetic materials) or superconductor- and-permanent magnet combinations (Bleuler, *et al*., 2009).

AMBs can actively be controlled, whereas PMBs cannot. For this reason AMBs are favoured above PMBs. AMBs are controlled using electromagnets, a feedback control loop, sensors, power amplifiers and other hardware and software (Bleuler, *et al*., 2009).

In contrast to AMBs, PMBs make use of permanent magnets only. It is physically impossible to have a purely passive suspension of a rigid body in all of its six degrees of freedom, using only permanent magnets ($\mu_r >> 1$) in a stationary configuration (Bleuler, *et al*., 2009). The system will always have at least one unstable degree of freedom according to Earnshaw's theorem (Bleuler, *et al*., 2009; Chen, *et al*., 1998).

Suspensions of this sort require the addition of gyroscopic forces or a dynamic controlling device or a force of different physical origin to stabilize the passive magnetic bearing arrangement (Bleuler, *et al*., 2009; Chen, *et al*., 1998). Stabilization can be achieved by using a mechanical bearing, an active electromagnet, and superconductor-to-magnet or diamagnet-to-magnet interactions (Bleuler, *et al*., 2009).

AMBs have also been used in PMB setups to stabilize the system by adding an AMB or AMBs to the PMB setup. Examples of such stabilization are found in turbo molecular pumps (Bleuler, *et al*., 2009). A disadvantage of PMBs is that they have very low damping. Mechanical or electromagnetic damping elements are necessary to provide suitable external damping forces required in the system. Thus AMBs are used to provide damping in a PMB setup (Bleuler, *et al*., 2009).

2.2 Research

The literature gathered in this study is covered under the following headings:

- Superconducting levitation
- Modelling

2.2.1 Superconducting levitation

The flux trapping effect of superconductors is temperature dependent as proven by Gruss *et al.* (2001) who found that at liquid nitrogen temperature, (77 K or -196.15 °C) the trapped field in pure YBCO was 0.8 T but at 57.9 K (-215.25 °C) the field was measured at 4.6 T (Gruss, *et al*., 2001).

Fuchs *et al.* (2005) conducted an experiment using bulk YBCO ($YBa_2Cu_3O_{7-x}$) disks of up to 50 mm in diameter to demonstrate the trapped field properties of the YBCO superconducting sample. The YBCO disk was cooled with liquid nitrogen. An external field was applied in the axial direction of the YBCO and then turned off. Pinned flux lines remained in the sample (Fuchs, *et al*., 2005).

A Hall sensor was used to scan the distribution of the trapped field in the superconductor. The maximum field $\boldsymbol{B_o}$ was found in the centre of the YBCO disks (Fuchs, *et al*., 2005). It was also found that this field increases with the critical current density and size of the disk. By chemical doping with Ag and Zn and neutron irradiation, improvements were made in flux pinning properties resulting in stronger levitation forces (Fuchs, *et al*., 2005; Gruss, *et al*., 2001; Fuchs, *et al*., 2003).

Fuchs *et al.* (2005) used an YBCO superconductor (34 mm diameter sample) and Sm-Co permanent magnet (25 mm diameter) to measure the force between the magnet and the superconductor. The YBCO was cooled at zero-field to 77K which for this case means that the YBCO sample was cooled at a distance far from the magnet (Fuchs, *et al*., 2005).

Fuchs *et al.* (2005) then reduced the distance between the magnet and superconductor which caused a repulsive force to develop because of the induced shielding current on the superconductor. A maximum levitation force of 100 N was measured at a small distance between the magnet and superconductor. The levitation pressure was 204 kPa over an area of approximately 491 mm^2 for this force at a distance of 2 mm between the magnet and superconductor (Fuchs, *et al*., 2005).

Experimental research that was conducted proved that the magnetic force between a magnet and a superconductor increases with a decrease in the distance between the magnet and superconductor (Chen, *et al*., 1998; Fuchs, *et al*., 2005; Neves, *et al*., 2002; Hauser, 1997; Fuchs, *et al*., 2003). A magnet levitating above a superconducting sample is stabilized laterally as well as vertically because of the forces caused by flux pinning (Fuchs, *et al*., 2005; Fedda, *et al*., 2007).

Levitation of a permanent magnet above YBCO thin films was successfully achieved by Schönhuber *et al.* (1994). Forces produced between the YBCO thin film and the magnet, were found to be lower than forces produced between bulk YBCO and the magnet. However, the magnet and the thin film combination had stronger lateral and vertical stiffness' compared to the bulk YBCO and magnet pair which were tested (Schönhuber, *et al*., 1994).

Chen *et al.* (1998) found that stronger levitation forces are obtained by using top seeded melt textured YBCO samples instead of sintered YBCO samples. Levitation forces with magnitudes of three orders higher were obtained by using top seeded melt textured YBCO samples, compared to levitation forces using sintered YBCO samples. Single grain crystal, melt textured grown YBCO samples also have superb magnetic shielding and field trapping capabilities (Chen, *et al*., 1998).

In a study of the performance of NdFeB and ferrite magnets in superconducting linear bearings with bulk YBCO samples, de Andrade Jr *et al.* (2003) found that NdFeB magnets produced magnetic forces an order of magnitude larger than that of ferrite magnets. The NdFeB magnets also produced greater magnetic stiffness compared to the ferrite magnets while levitating above a bulk YBCO rail (de Andrade Jr., *et al*., 2003).

2.2.2 Modelling

To analyse forces obtained in superconducting levitation, modelling has been done by means of numerical calculations and finite element methods, using code and programming algorithms.

Neves *et al.* (2002) used the finite element method (FEM) and the Bean Critical State Model (BCSM) to simulate the levitation force between a permanent magnet and a superconductor. ANSYS MULTIPHYSICS 5.7 was used to calculate the levitation force in two dimensions. The forces from the simulation were then compared to actual measured forces (Neves, *et al*., 2002).

Neves *et al.* (2002) found that for small air gaps of 5 mm or less, the simulated force curves and the experimental measured force curves were in agreement. However for air gaps larger than 20 mm the simulated force curves deviated from the experimental measured force curves (Neves, *et al*., 2002).

Figure 11 is a representation of the simulated magnetic flux density which was obtained by Neves *et al.* (2002). The magnetic flux did not penetrate the superconductor as the superconductor repelled the flux clearly demonstrating the Meissner effect.

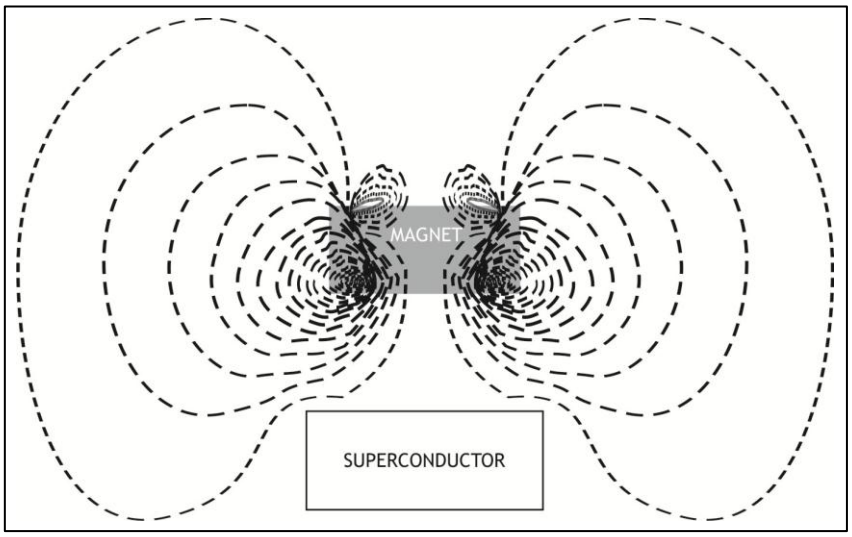

Figure 11: Schematic of magnetic field and superconductor interaction. The magnetic field of the magnet is repelled by the superconductor and does not penetrate the superconductor at all (Modified after Neves, *et al*., 2002).

Hauser (1997) made use of the ANSYS-code to determine the forces generated between a superconductor and a magnet. To consider partial flux penetration in FEM analyses, Hauser (1997) suggested setting the relative permeability to a value between 0 and 1 for the superconductor in the simulations.

Hauser (1997) also assumed a very high electrical conductivity for the superconductor in finite element code to consider partial flux penetration. Partial flux penetration is referred to as the non-perfect diamagnetic model. The perfect diamagnetic model is based on the assumption of complete flux penetration. Hauser found that using the non-perfect model in

calculations gave partial good agreement of curves for force versus distance between measured and calculated data (Hauser, 1997).

Hauser (1997) developed a user element for the ANSYS code which was used to solve for the forces between a superconducting disk and a disk magnet which would obtain better results than using the non-perfect diamagnetic model in calculations. The element named SUPRA105 was written to include three models for the electromagnetic behaviour of an HTSC and magnetic field dependencies for the critical current density $\boldsymbol{J_c(B)}$ (Hauser, 1997).

The three models that are included in the SUPRA105 element, according to Hauser (1997), are:

- Bean model, $\boldsymbol{J_c(B)} = C$
- Kim model, $\boldsymbol{J_c(B).(B_0 + B)} = C$
- Matsushita model, $\boldsymbol{J_c(B)} = \boldsymbol{J_{c0}.B^{-1/2}}$

The SUPRA105 element was then used with the critical state model and the frozen field model respectively to calculate the forces between the superconductor and magnet. The frozen field model and critical state model are existing superconductor models (Hauser, 1997).

According to Hauser (1997) the critical state model gives good results for the calculation of levitation force. It is also stated that the critical state model is used to evaluate large levitation forces between a bulk HTSC and a magnet (Tsuchimoto, 2001). Hauser (1997) gives the critical state model as:

$$\boldsymbol{J} = \boldsymbol{J_c}(|\boldsymbol{B}|).\frac{\boldsymbol{E}}{|\boldsymbol{E}|}\ for\ |\boldsymbol{E}| \neq 0$$

$$\frac{\partial \boldsymbol{J}}{\partial t} = 0\ for\ |\boldsymbol{E}| = 0$$

According to Hauser (1997) the frozen field model is used to calculate the levitation forces and can handle horizontal restoring forces as well. Tsuchimoto (2001) states that the frozen field model is based on an assumption that fluxoid are fixed at pinning points on the surface of the HTS. Tsuchimoto (2001) also used the frozen field model to evaluate the stiffness of horizontal restoring force between a bulk superconductor and magnet. Hauser (1997) gives the frozen field model as:

$$\boldsymbol{J} = \boldsymbol{J_c}(|\boldsymbol{B}|).\frac{\boldsymbol{E}}{|\boldsymbol{E}|}\ for\ |\boldsymbol{F_l}| > \boldsymbol{F_p}$$

$$\frac{\partial \boldsymbol{J}}{\partial t} = 0 \; for \; |\boldsymbol{F_l}| \leq \boldsymbol{F_p}$$

where $\boldsymbol{F_l}$ (N) is the local force acting on the fluxoid, $\boldsymbol{J_c}$ is the superconducting critical current density (A/m^2) and $\boldsymbol{F_p}$ (N) is the pinning force.

Hauser (1997) stated that results obtained from simulations using the critical state model and frozen field model with the SUPRA105 element clearly corresponded to measured results that were obtained from experimental tests conducted by Hauser (1997).

According to Chen *et al.* (1998) the force between a zero-field cooled superconductor and a magnet is given by

$$\boldsymbol{F} = \int \boldsymbol{J_c} \times \boldsymbol{B} dV \qquad \textbf{(15)}$$

where $\boldsymbol{F}$ is the force (N), $\boldsymbol{B}$ is the flux density (T) and V is the volume (m^3). Chen *et al.* (1998) proved that stronger levitation forces are obtained by increasing the external magnetic flux density and increasing the volume of the superconductor.

Chen *et al.* (1998) stated that an analytical solution of Equation 15 for forces between a disc-shaped permanent magnet and a superconductor is not readily available. This was ascribed to the non-uniform magnetic field and the current density which is a function of the applied field. However Chen *et al.* (1998) easily measured the forces between a magnet and a superconductor by experimental studies.

Chen *et al.* (1998) found that the levitation force is increased by increasing the field cooling gap for a superconductor and magnet while cooling the superconductor. However the stability or lateral stiffness decreased as the field cooling gap was increased.

The field cooling gap is the air gap between the superconductor and magnet while the superconductor is cooled and the distance at which the permanent magnet levitates after being pinned. Masses between 2.5 kg and 4 kg could be levitated for different magnet and superconductor configurations (Chen, *et al*., 1998).

Chen *et al.* (2001) presented an empirical method to calculate the magnitude of the forces between a disc-shaped permanent magnet and a superconductor. Chen *et al.* (2001) states that the current density $\boldsymbol{J_c(r,z)}$ of the current induced by the magnet's applied field of the superconductor can be divided into two parts. The first part is the current density on the surface, $\boldsymbol{J_{s,s}}$ and the second part is the volume current density $\boldsymbol{J_{v,s}}$ (Chen, *et al*., 2001).

Both these current densities are used to determine the surface, $\boldsymbol{B_{s,z}}$ and volume, $\boldsymbol{B_{v,z}}$ magnetic flux densities of the superconductor in the z-axis. A third current density exists on the surface of the permanent magnet $\boldsymbol{J_{s,m}}$. This is because the magnetic flux density of the

permanent magnet can be treated as a ring of surface current which has a surface current density $\boldsymbol{B_{r,m}}$ (Chen, *et al*., 2001).

According to Chen *et al.* (2001) the magnetic levitation force is calculated as the interaction force between the currents on the superconductor and the currents on the magnet. Thus the force is given by the summation of the forces caused by the interaction of the flux density of the magnet and the $\boldsymbol{J_{s,s}}$ (surface current density) and $\boldsymbol{J_{v,s}}$ (volume current density) terms of the superconductor which are given as $\boldsymbol{F_{z,s}}$ and $\boldsymbol{F_{z,v}}$ respectively:

$$F_{z_s} = \alpha_z \int_h^{h+t_s} \int_0^{2\pi} b_s J_{s,s} B_{r,m} d\phi dz$$

$$F_{z_v} = \alpha_z \int_{b_1}^{b_2} \int_h^{h+t_s} \int_0^{2\pi} r J_{v,s} B_{r,m} d\phi dz dr$$

where r, ϕ and z represent the coordinates in a cylindrical coordinate system, h and t represent the thickness of the superconductor and magnet, α_z is a directional vector and b_1 to b_2 is the region along the r axis on the superconductor (Chen, *et al*., 2001).

Perini *et al.* (2009) used the E-J power law to develop a numerical model for the superconductor material. The equation is given by

$$\boldsymbol{E} = \boldsymbol{E_0} \left(\frac{\|\boldsymbol{J}\|}{\boldsymbol{J_c}(\boldsymbol{B}, T)} \right)^{n(\boldsymbol{B},T)} \frac{\boldsymbol{J}}{\|\boldsymbol{J}\|}$$

where $\boldsymbol{E}$ is the electric field, $\boldsymbol{E_0}$ is the electric field at the time $t = 0$, $\boldsymbol{J}$ the current density, $\boldsymbol{J_c}$ the critical current density, $\boldsymbol{B}$ the magnetic field and T the temperature (Perini, *et al*., 2009). Perini *et al.* (2009) successfully validated the data obtained from the numerical model with the experimental data for the levitation of a magnet above an MgB_2 disk superconductor.

Fedda *et al.* (2007) derived three mathematical equations to calculate the levitation force between a small magnet and a superconducting ring using a dipole-dipole interaction model. Fedda *et al.* (2007) found that the levitation force on the magnet increased to a maximum when the distance between the magnet and centre of the ring was decreased. The force then decreased to zero when the magnet was moved to the centre of the ring (Fedda, *et al*., 2007).

The magnet was defined as a single magnetic dipole that levitates at a distance h from the centre of the superconducting ring. Fedda *et al.* (2007) also assumed that the magnetic moment of the dipole was 0.001 Am^2. Field cooling and zero field cooling were not considered in the model. Figure 12 is a schematic representation of the magnetic dipole

and superconducting ring model, for which the equations presented below were derived for (Fedda, *et al*., 2007).

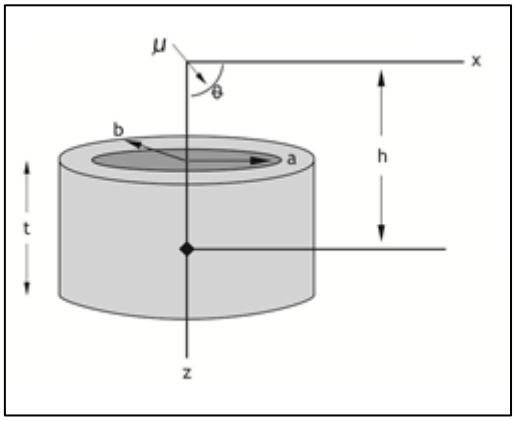

Figure 12: Schematic of the superconductor ring and the magnetic dipole (μ) at angle θ for which Fedda *et al*., (2007) derived the equations listed (Modified after Fedda *et al*. 2007).

The three equations were derived for three special cases. Each case is given with its corresponding equation below (Fedda, *et al*., 2007):

1. A superconducting ring has an infinite outer radius (*b* = ∞). The force is calculated in the limit, $\lim_{b\to\infty} F$ which gives the equation:

$$\boldsymbol{F} = \frac{2\mu_0\mu^2 ht[384a^6+336a^4B_1+9B_2^2B_1+32a^2B_3-3(128a^6+128a^2h^2t^2+48a^4B_1-B_2^2B_1)cos2\theta]}{\pi(4a^2+(-2h+t)^2)^3(4a^2+(2h+t)^2)^3} \quad \textbf{(16)}$$

2. A superconducting ring for which the inner radius approaches zero. The force is calculated in the limit, $\lim_{a\to 0} F$, as:

$$\boldsymbol{F} = \frac{12\mu_0\mu^2 htB_1(1+\cos^2\theta)}{\pi B_2^4} \quad \textbf{(17)}$$

3. A superconductor that is very thin. The superconductor is much thinner than what the distance is from which the dipole levitates from the superconductor's centre (*t* << *h*) and gives:

$$\boldsymbol{F} = \frac{3\mu_0\mu^2 t(1+\cos^2\theta)}{16\pi h^5} \quad \textbf{(18)}$$

with $B_1 = 4h^2 + t^2$, $B_2 = -4h^2 + t^2$ and $B_3 = 48h^4 + 4^2t^2 + 3t^4$.

According to Fedda *at al.* (2007) calculated results were in good qualitative agreement with experimental results. Fedda *et al.* (2007) also found calculated results to be in agreement with the experimental results for the forces between a small magnet and superconducting

ring obtained by Ma *et al.* (2001). In these experiments the superconductor was field cooled and zero-field cooled and the forces were measured between the magnet and superconductor (Ma, *et al*., 2001).

2.3 Summary

A background on superconductivity and superconducting levitation fundamentals has been given in the preceding chapters, however much literature has been gathered on levitation capabilities of superconductors and the improvement thereof. Investigation has also been conducted on levitation force determination between magnets and superconductors. However, during the course of the literature study no literature could be found on superconducting levitation as suspension mechanism in cryogenic storage containers.

After considering the research in the literature study it was only logical to investigate the technology and the phenomenon of superconducting levitation in concepts of cryogenic containers for the stable suspension of a liquid hydrogen container within another, to reduce thermal conductivity in a non-filling or delivery state of the stored H_2.

2.4 Purpose of study

The purpose of this study now is to suggest a concept for the storage of liquid hydrogen, typically for vehicular transport applications, in which an inner vessel is magnetically suspended in a vacuum drawn outer vessel. It is also the purpose of this study to validate the concept, by determining the magnitude of forces obtainable between magnets and superconductors in the superconducting state. In this study no attempt will be made to evaluate the influence of the above mentioned on filling and delivery to the container.

Chapter 3: Conceptual design

In Chapter 1 arguments were presented that liquid hydrogen can be stored in a container of lesser volume than the storage volume required for storage of compressed gaseous hydrogen of equal amount. It was also argued that if liquid hydrogen storage is pursued, heat transfer from the environment to the hydrogen should be reduced to a minimum.

As discussed in Chapter 1, there are different container patents that exist for hydrogen storage which limit heat transfer to the hydrogen. However unacceptable heat transfer from the environment to the hydrogen still occurs through physical supports, which leads to hydrogen boil-off. These losses can be reduced by possibly magnetically suspending an inner container within another container and thereby eliminating the use of physical supports.

In an attempt to reduce hydrogen boil-off, a conceptual design for storage of liquid hydrogen is presented and discussed for which superconducting levitation is suggested as magnetic suspension mechanism between an inner- and outer container. The focus of the conceptual design is a first approximation of the feasibility of magnetic suspension of said container concept and not of the container itself. It should also be noted that for this study the effects of the inlet/outlet pipe are ignored.

A CAD model of the conceptual design is presented in Figure 13. The CAD model in Figure 13 depicts a double wall cryogenic container concept for liquid hydrogen storage in vehicular transport applications. For the CAD model the walls of the inner and outer vessels are transparent to display support frames in which magnets and superconductors are mounted for levitation purposes.

The concept represented by the CAD model in Figure 13 is designed for a medium size four seat passenger vehicle with a 118 kW engine, such as a Volkswagen Golf (© Volkswagen, 2012). The average travelling speed of the vehicle is 120 km/h and the travel distance is 480 km (USDOE requirements). It is calculated that approximately 14.2 kg L-H_2 is sufficient to travel 480 km and that a container with a storage volume of approximately 200 l (0.2 m^3) is required (deduced from Figure 1).

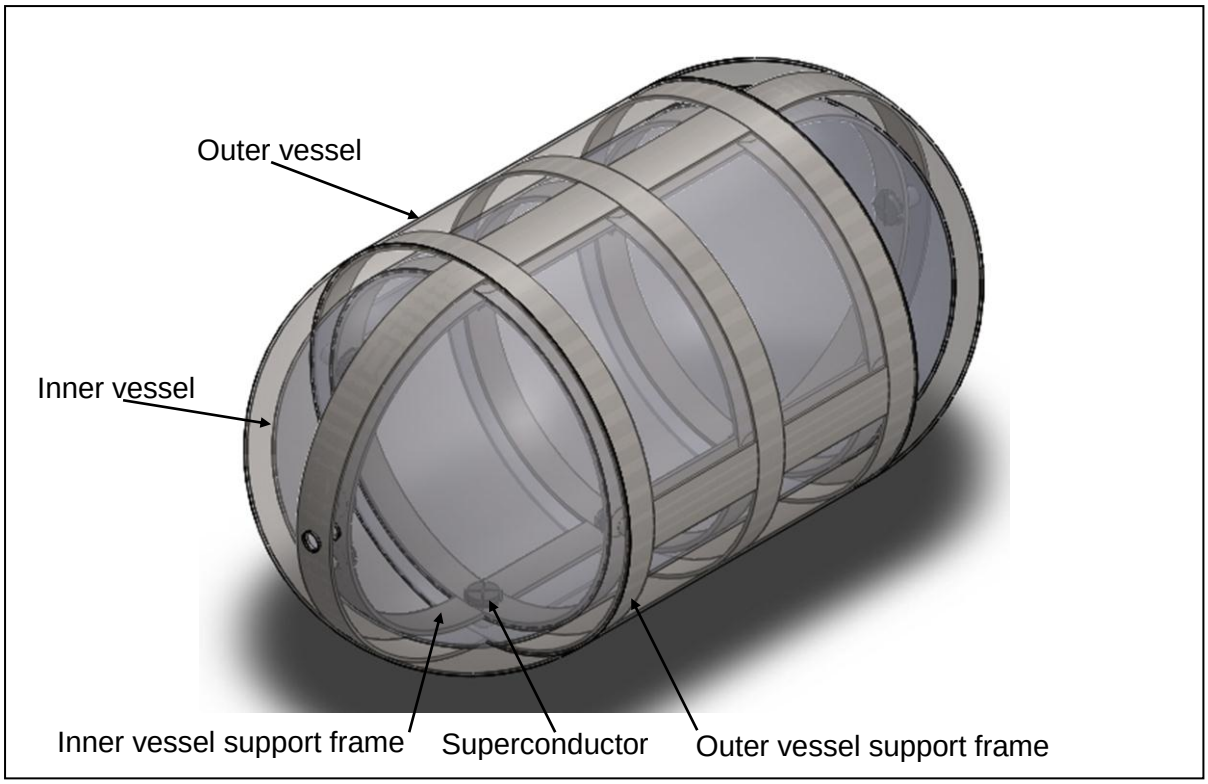

Figure 13: Isometric view of a CAD model of the double wall cryogenic container concept for liquid hydrogen storage in vehicular transport in which suspension of the inner vessel is achieved by electromagnetic- and superconducting levitation.

For calculations concerning the design of the container presented in Figure 13, refer to the EES Code in Appendix B. The hydrogen container concept presented in Figure 13 is covered under the following headings:

- Outer vessel and connected parts
- Inner vessel and internals
- Magnetic suspension

3.1 Outer vessel and connected parts

The outer vessel and connected parts consist of:

- Electromagnet
- Outer vessel
- Outer vessel support frame
- Permanent magnets
- Magnet caps

3.1.1 Electromagnet

An electromagnet is used to levitate the inner container within the outer container. The electromagnet which is an air coil (magnet has no metal core) is positioned below the outer vessel centre as presented in the section view of the CAD models in Figure 14. The electromagnet has 500 turns of copper wire of 0.0007 mm thickness and has a core cross sectional diameter of 0.1 m.

The electromagnet is designed to run at 220 V with a 14 A alternating current which induces a magnetic field with strength of 362.5 kA/m. It is designed to provide a lift force of approximately 660 N, which is to lift approximately 66 kg. The force deliverable by the electromagnet is above the required force of 610 N, as the filled inner vessel with internals weighs approximately 62.2 kg. For simplicity reasons the electromagnet is presented as a round solid disk in Figure 14.

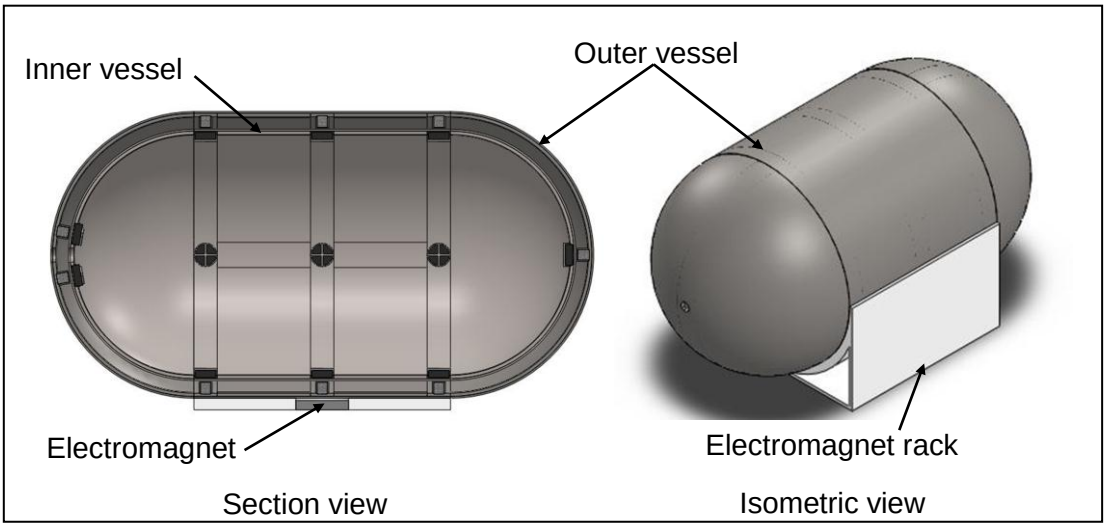

Figure 14: CAD models of a section view and an isometric view of the electromagnet mounted in its rack below the outer vessel centre.

The electromagnet is secured in a rack which holds it in place beneath the centre of the outer vessel. The design of the rack is not of interest for this study as the focus is on the magnetic suspension mechanism. For this reason it is not further discussed.

3.1.2 Outer vessel

A CAD model of the outer vessel is presented in Figure 15. The outer vessel is a cylindrical storage vessel with hemispherical end caps. It is designed to be positioned horizontally in a vehicle and to encapsulate the inner vessel as well as a support frame. Permanent magnets are mounted in the support frame for levitation purposes. A medium vacuum of 1 kPa is

drawn in the outer vessel to reduce convection between the two vessels and ultimately to reduce hydrogen boil-off (NPL Management Limited, 2012).

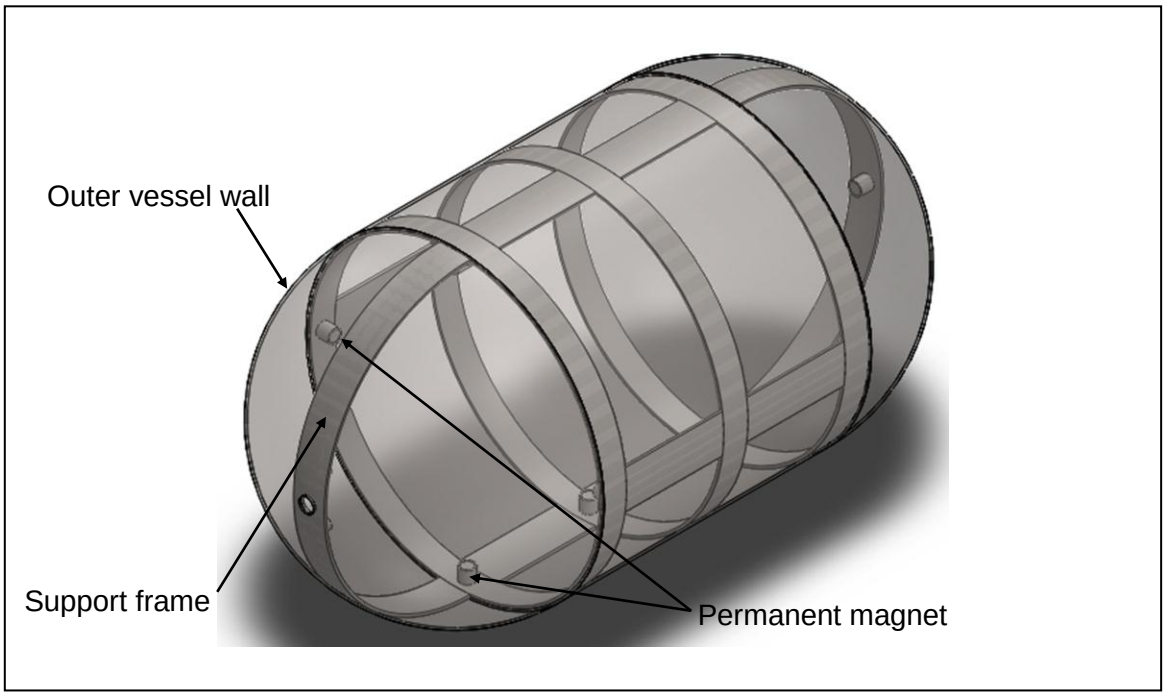

Figure 15: Isometric view of a CAD model of the outer vessel and connected parts.

The inner diameter of the outer vessel is approximately 0.606 m and the length of the vessel is approximately 1.16 m. The wall thickness of the outer vessel is 4 mm. 304L stainless steel is the selected material for the outer vessel wall as it is used for cryogenic storage applications (MatWeb, LLC, 2012). 304L stainless steel also has a high weldability which ensures ease of joining the vessel and support frame parts.

304L stainless steel is ferromagnetic and due to its magnetic permeability ($\mu = 1.008$) it increases the magnetic flux density (***B***) produced by the electromagnet as discussed in Chapter 2.1.1, derived from Equation 3. The stronger magnetic field in turn produces a stronger magnetic force when the inner vessel is levitated by the electromagnet at the initial filling of the container. The levitation of the inner container is discussed in Chapter 3.3.1.

3.1.3 Outer vessel support frame

In Figure 15 the vessel wall of the CAD model is transparent to show the outer vessel support frame which is encapsulated in, and welded to the vessel. A CAD model of a section view of the support frame is presented in Figure 16.

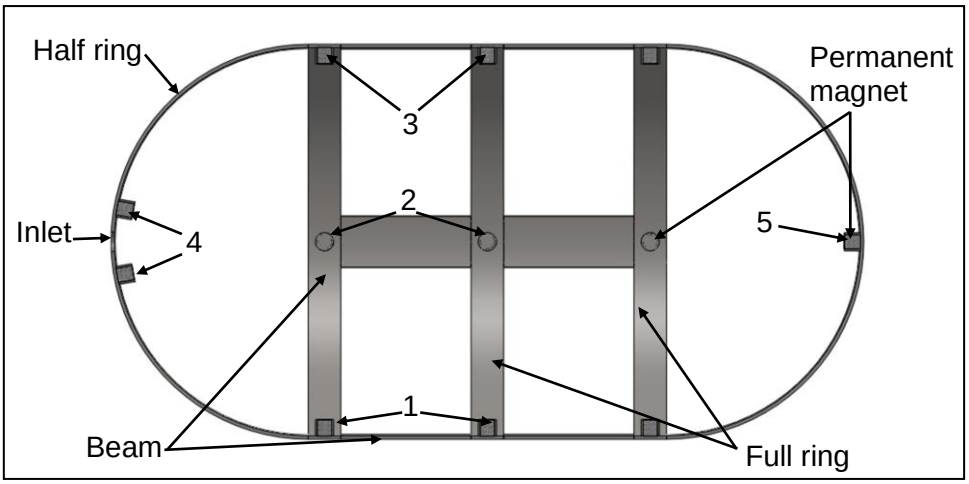

Figure 16: Right sectioned view of the CAD model of the outer vessel support frame which holds permanent magnets.

The frame consists of three parallel rings that are adjoined by beams with half rings that in turn are joined to each of the outer rings. Permanent magnets are mounted in the rings and half rings of the support frame for levitation purposes as discussed in Chapter 3.3.1. The support frame is also made from 304L stainless steel for the same reasons stated as for the use of 304L stainless steel for the outer vessel wall.

3.1.4 Permanent magnets

The permanent magnets provide magnetic flux which is trapped in the superconductors (situated in the inner container support frame) to achieve levitation and ultimately suspension of the inner container within the outer container. The permanent magnets are secured in holes in the rings (Figure 17: Isometric view) with magnet caps which are welded to the ring. Figure 17 also presents a close up view of a magnet cap securing a permanent magnet in a hole.

In the section view of the CAD model presented in Figure 16, the magnets on the bottom of the rings (those numbered 1) are the magnets that produce the levitation force that levitates the inner vessel once the magnetic fields are pinned in the corresponding superconductors, ultimately providing magnetic suspension. There are three such magnets.

The magnets on the top, left and right parts of the rings (numbered 2 through 5) provide a constraint on the inner vessel prohibiting it from moving around in the outer vessel once the magnetic fields are pinned in corresponding superconductors. The magnets are 22 mm in diameter and 25 mm long.

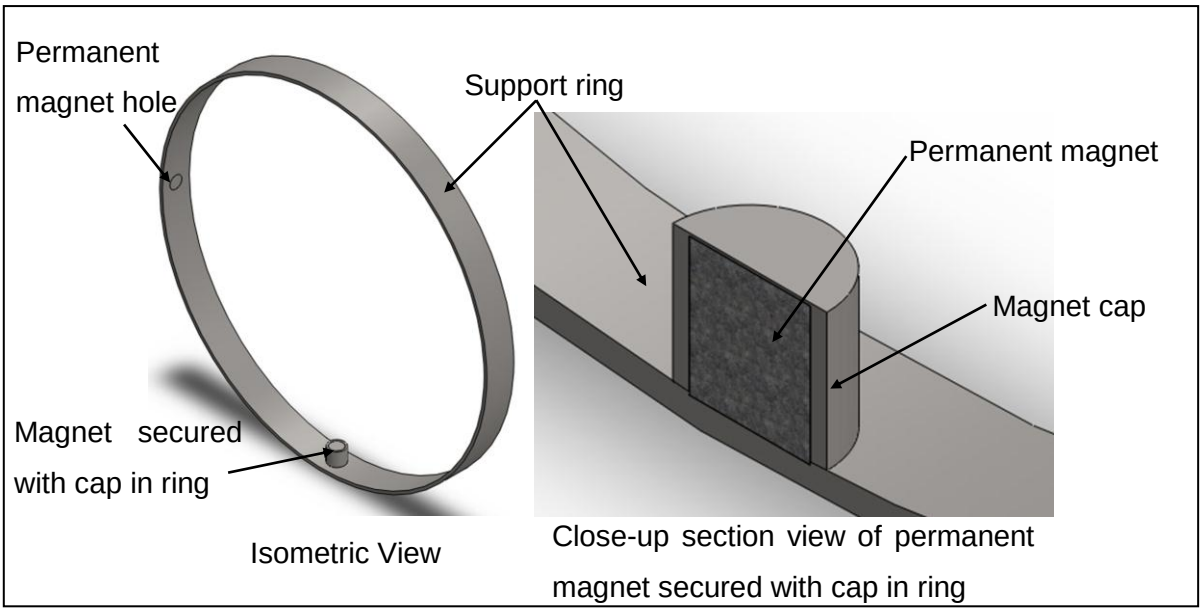

Figure 17: CAD models of an isometric view and a close up section view of a permanent magnet mounted in a ring.

The strongest magnetic forces possible are required for the levitation of the inner vessel. High magnetic stiffness is also required for the suspension system as this determines the movement of the inner vessel in the outer vessel if there is any disturbance force that acts on the container setup. An example of a disturbance force is when the vehicle drives over a bump in the road, which causes the inner vessel to move within the outer vessel.

Due to the findings of De Andrade Jr *et al.* (2003) mentioned in the literature survey that NdFeB magnets produce magnetic forces of an order larger than that of ferrite magnets and that NdFeB magnets have greater magnetic stiffness' than ferrite magnets while levitating above a bulk YBCO rail, NdFeB magnets were selected above sintered magnets for this concept.

These magnets are N37 neodymium magnets. The N in the name shows that the magnet is made from neodymium (NdFeB Specialists E-Magnets UK Limited, 2011). The number following the N is the (BH)max (maximum energy product) given in MGOe (Mega Gauss-Oersted). The corresponding residual induction ($\boldsymbol{B_r}$) of a N37 magnet is 1.24 T (Sable Magnetics, 2011).

3.1.5 Magnet caps

The magnet caps are small hollow cylindrical shells that fit over the magnets and are welded to the rings to secure the magnets in position. The caps also protect the magnets from being damaged by the container when it rests on the caps before it is levitated and filled.

The magnet caps are made from 304L stainless steel and due to the fact that it is a ferromagnetic material the caps align the magnetic field of the magnet directing it at the superconductor. Figure 18 is a CAD model of an isometric sectioned view of the magnet cap.

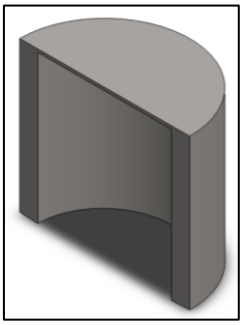

Figure 18: Sectioned isometric view of a CAD model of the permanent magnet cap.

Should the suspension fail, that is if the hydrogen is depleted and the superconductors' temperature rise above T_c causing breakdown of the pinning effect, the caps would also protect the magnets from impact by the inner vessel.

3.2 Inner vessel and internals

The inner vessel and internals consist of:

- Inner vessel
- Inner vessel support frame
- Superconductors
- Support cap

3.2.1 Inner Vessel

Figure 19 presents a CAD model of the inner vessel in isometric view. The inner vessel is a cryogenic capable cylindrical storage vessel with hemispherical end caps designed to store the required 14.2 kg liquid hydrogen at sub-cooled temperature (20 K) and high pressure (10 MPa).

To satisfy the 200 l (0.2 m^3) volume requirement the inner vessel is designed with a total length, inner diameter and wall thickness of approximately 1.1 m, 0.53 m and 4 mm respectively. Due to the 4 mm wall thickness the vessel occupies a space of approximately 210 l (0.21 m^3) and weighs approximately 33 kg because of the density of Ti-5Al-2.5Sn ELI (4480 kg/m^3) (Collings, 1994).

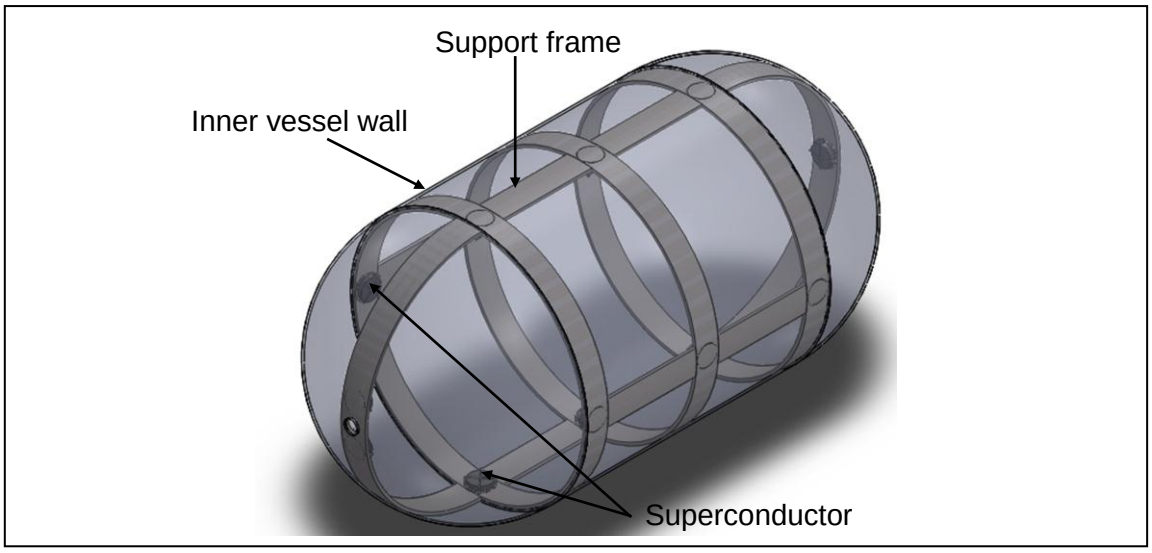

Figure 19: Isometric view of a CAD model of the inner vessel and internals.

To safely store liquid hydrogen the vessel wall is made of Ti-5Al-2.5Sn ELI, a material which is used in cryogenic pressure vessels. Ti-5Al-2.5Sn ELI is a paramagnetic material and due to the alternating current in the electromagnet it will levitate above the electromagnet within the outer vessel. This is based on the magnetic levitation principal discussed in Chapter 2.1.4, in which an electromagnet levitates above a paramagnetic plate.

Due to the paramagnetic behaviour, the material has no effect on the permanent magnets' magnetic fields and will not disrupt the levitation forces or affect the suspension of the inner vessel. Due to good weldability of the material, the vessel and internal parts are easy to join.

3.2.2 Inner vessel support frame

For the inner vessel concept presented in Figure 19 the vessel wall is transparent to show the inner vessel support frame which is encapsulated in the vessel. A CAD model of a section view of the support frame is presented in Figure 20.

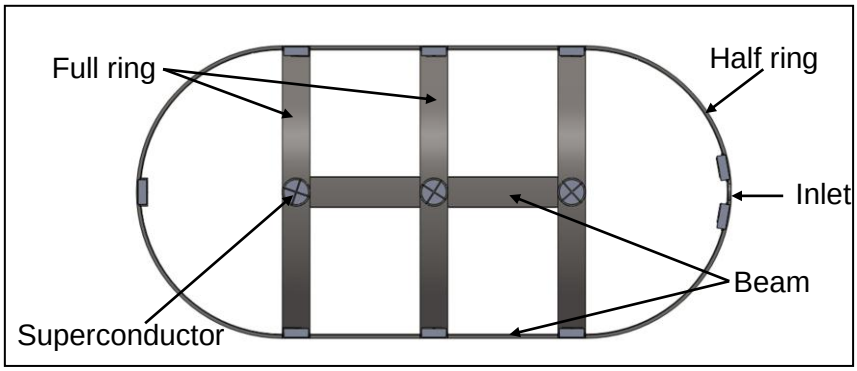

Figure 20: Right sectioned view of the CAD model of the inner vessel support frame which holds superconductors.

Similar to the outer vessel support frame, the inner vessel support frame also consists of three parallel rings (Figure 20), adjoined by beams with half rings joined to each of the outer rings. However, instead of permanent magnets, superconductors are mounted in the rings and half rings of the support frame for magnetic suspension purposes. The support frame is also made from Ti-5Al-2.5Sn ELI. Due to the density of the material the approximate mass of the frame is 13 kg.

3.2.3 Superconductors

Superconductors are used to pin the magnetic fields produced by the magnets to levitate the inner container within the outer container. The pinning phenomenon occurs once the superconductors are cooled below T_c, with the liquid hydrogen that is pumped into the container to be stored. The superconductors are secured with superconductor caps in holes in the rings as presented in Figure 21.

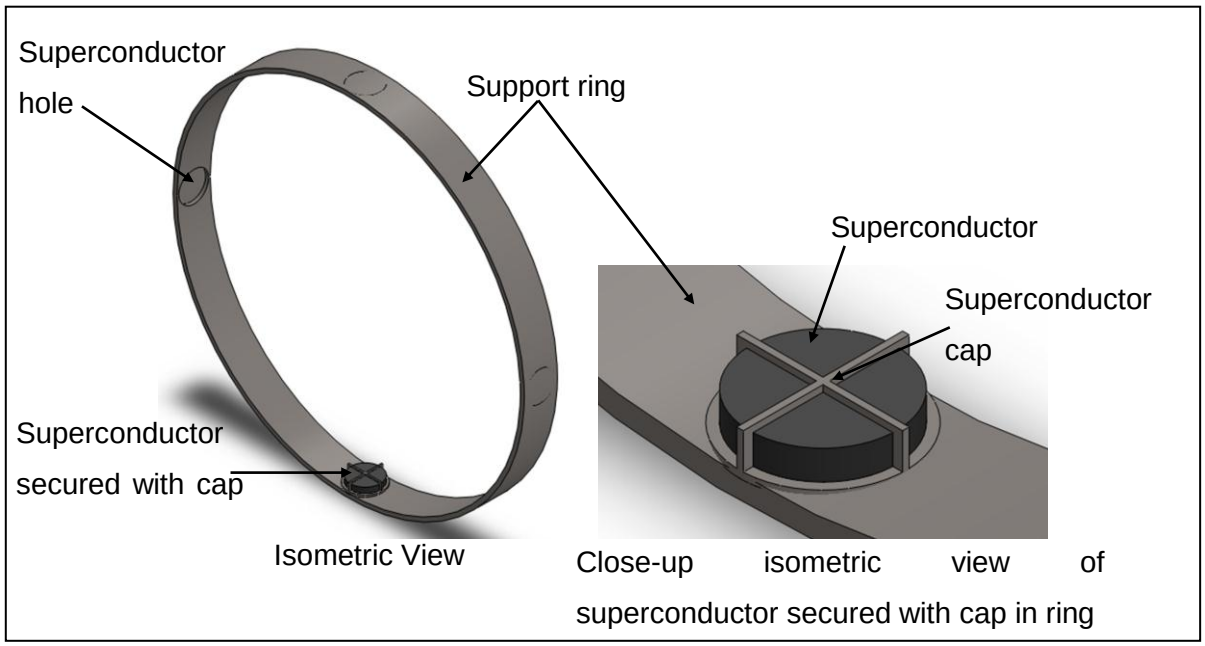

Figure 21: CAD models of an isometric view and a close up isometric view of a superconductor mounted in a ring.

The strongest levitation forces possible are required for the levitation of the inner vessel. As mentioned in the literature survey, Chen *et al.* (1998) found that stronger levitation forces are obtained by using top seeded melt textured YBCO superconductors compared to sintered YBCO superconductors. Chen *et al.* (1998) also found that levitation forces with magnitudes of three orders higher were obtained by using top seeded melt textured YBCO samples, compared to levitation forces using sintered YBCO samples.

It was discovered by Chen *et al.* (1998) that single grain crystal, melt textured grown YBCO samples also have superb magnetic shielding and field trapping capabilities. Based on the findings of Chen *et al.* (1998), which are discussed in the literature study, single grain top seeded melt textured circular YBCO disks of 45 mm diameter and 16 mm thickness were selected for this concept design.

3.2.4 Superconductor cap

Once the superconductors are secured with the caps in the holes of the rings they are welded to the rings. The superconductor caps are made with cavities as seen in the CAD model presented in Figure 22. It is done so to insure that the superconductor cools uniformly, trapping a uniform magnetic field in the superconductor for stable levitation and better pinning forces.

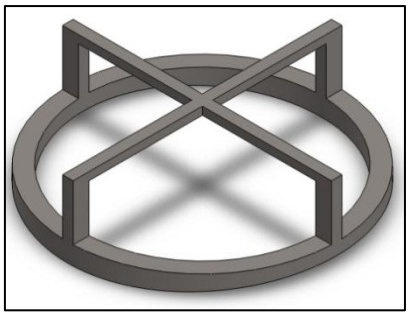

Figure 22: Isometric view of a CAD model of the superconductor cap.

The cavities also ensure an increase in the cooling rate of the superconductor because there is direct contact between the liquid hydrogen and most of the superconductor surface. The superconductor cap is also made from Ti-5Al-2.5Sn ELI.

3.3 Magnetic suspension

Magnetic suspension of the inner vessel within the outer vessel is discussed under the following headings:

- Suspension mechanism
- Mathematical study
- Finite element study
- Summary

3.3.1 Suspension mechanism

Magnetic suspension of the inner vessel is achieved by two forms of magnetic levitation. The first is electromagnetic levitation for which an electromagnet provides the required force to levitate the inner vessel whilst liquid hydrogen is being pumped into the vessel. The second is by means of forces generated by the interaction between superconductors in the superconducting state and the magnetic fields of permanent magnets, for which the magnetic fields are pinned in the superconductors.

To magnetically suspend the inner vessel, an electromagnet (discussed in Chapter 3.1.1) driven by an alternating current is used to supply a magnetic field which induces eddy currents in the vessel wall and in turn induces an opposing magnetic field in the paramagnetic inner vessel wall. This is done to position the inner vessel and outer vessel so that the superconductors and permanent magnets, in their respective support frames, are positioned with a 10 mm levitation gap (air gap) in a concentric position.

As electromagnetic suspension takes place the inner vessel is filled with liquid hydrogen, which in turn cools the superconductors below their T_c and induces the superconducting state. The superconductors then pin the magnetic fields of the permanent magnets. The field of the electromagnet is also pinned in the superconductor, but does not affect superconducting levitation as the electromagnet is switched off once the magnetic fields of the permanent magnets are pinned.

Figure 23 is a close up sectioned view of a CAD model of a superconductor and a permanent magnet secured in a concentric position 10 mm apart. Both magnet and superconductor are secured in their respective support frames within their vessels by use of magnet- and superconductor caps. There is a 3 mm gap between the inner vessel wall and the magnet caps if the inner vessel moves as the vehicle drives over a bump.

The levitation force that works on the superconductors causes the superconductors to levitate which in turn causes the support frame within the inner vessel to levitate resulting in the levitation of the inner vessel because the superconductors are secured to the frame with superconductor caps.

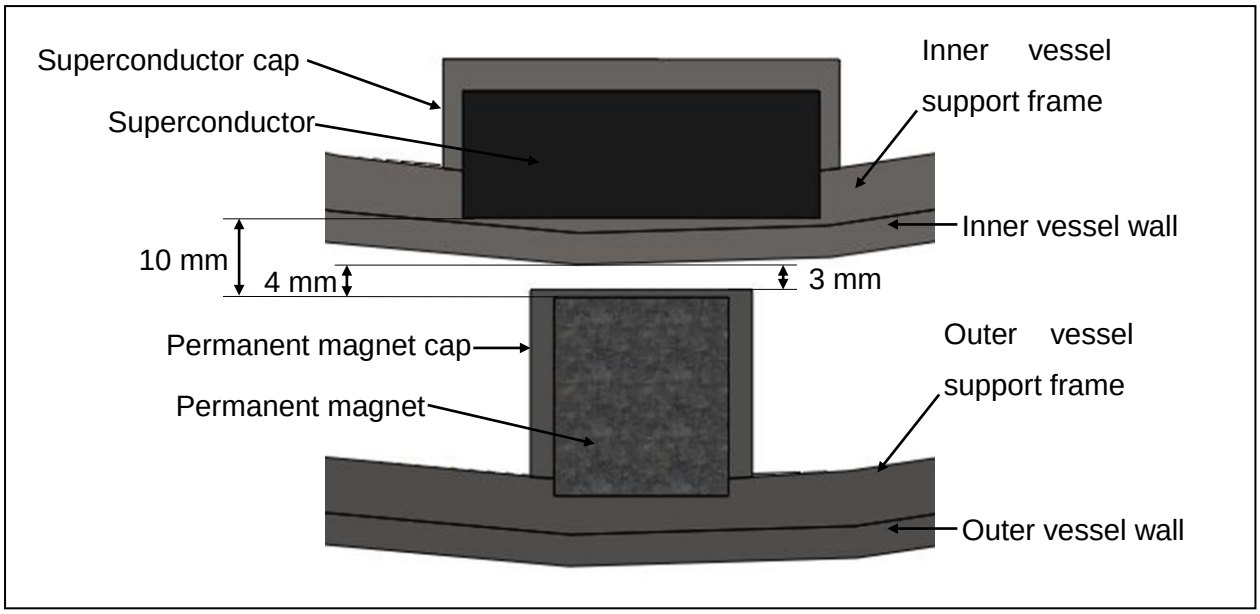

Figure 23: Close up frontal sectioned view of a CAD model of a superconductor and magnet mounted their specific support frames within their specific containers with an air gap of 10 mm between the magnet and superconductor.

To levitate the filled inner container by means of superconducting levitation, a permanent magnet is required which delivers a magnetic force of 610 N. Equation 14 was used to calculate the appropriate size of a magnet required in combination with a superconductor in the superconducting state to levitate the inner vessel.

It was calculated that a magnet of approximately 36 mm in diameter is required to levitate the total mass of the filled container. The possible instability of the container levitated by only one magnet is countered by the addition of more magnets to produce the levitation force required to levitate the inner vessel.

It was therefore decided that three smaller magnets would suffice to provide the required levitation force, by adding the forces delivered by the magnets. To determine the size of the smaller magnets the total force required to lift the inner container was divided by three. With the use of Equation 14, the required size of the smaller magnets was calculated at approximately 22 mm diameter. According to calculations these smaller magnets each produce a force of approximately 203 N.

However Equation 14 cannot be used to calculate the forces between a magnet and superconductor as a function of the air gap because it is derived for the maximum force a magnet can deliver and does not consider the distance between the superconductor and magnet.

Due to the fact that Equation 14 cannot be used to determine the forces as function of the air gap the forces between the magnet and superconductor were determined mathematically using the equation derived by Fedda *et al.* (2007) (Equation 17) and by finite element modelling and simulations using ANSYS Multiphysics. The mathematical study and finite element study on the forces between a superconductor in the superconducting state and a permanent magnet are discussed in the following paragraphs.

3.3.2 Mathematical study

Fedda *et al.* (2007) used Equation 17 to calculate the forces between a small magnet and a ring shaped superconductor in the superconducting state by modelling the magnet as a single magnetic dipole. To determine the forces between the 22 mm diameter magnet and the superconductor of this study, Equation 17 derived by Fedda *et al.* (2007) was used. The EES code used to solve Equation 17 is given in Appendix C.

Fedda *et al.* (2007) made the assumption that the magnetic moment of the magnet dipole is [1]$\mu = 0.001\ Am^2$. For this study the same assumption was made. The magnitude of the force was calculated for different distances (air gaps) between the superconductor and the magnet. The air gaps ranged from 0.1 mm to 10 mm because at 0 mm air gap the equation could not solve because it resulted in a division by zero.

Table 1: Calculated forces between the magnet and superconductor for air gap intervals from 0.1 mm to 10mm.

Force (N) Calculated	Air gap (mm)	0.1	1	2	3	4	5	6	7	8	9	10
	Force (N)	375.0	4E-02	2E-03	5E-04	1E-04	6E-05	3E-05	2E-05	9E-06	6E-06	4E-06

At 0.1 mm air gap, the force between the superconductor and magnet was calculated as approximately 375 N. This is equivalent to levitating a mass of approximately 38 kg. As the air gap increases from 0.1 mm to 10 mm the force between the magnet and superconductor decreases. The relationship between the force and air gap is presented in Figure 24.

[1] The symbol μ is also used to denote the magnetic moment of a material as well as the permeability of a material. However the units in which these two properties are measured differ.

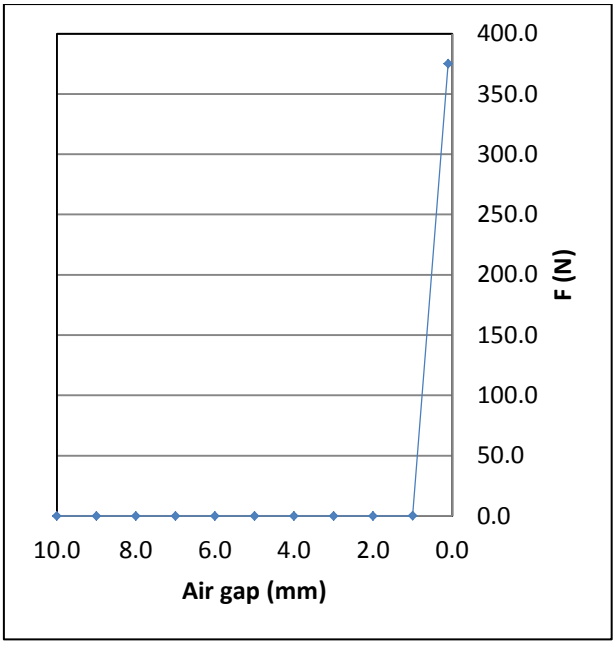

Figure 24: Graph of the relationship between levitation force and air gap obtained by calculations.

3.3.3 Finite element study

A finite element (FE) study was conducted to determine the magnitudes of force between a superconductor and a 22 mm diameter magnet. SolidWorks was used to draw geometry for the FE model. ANSYS Multiphysics is the finite element software that was used in the FE study. The geometry that was drawn in SolidWorks was imported into the geometry component in ANSYS Multiphysics' Workbench interface.

The magnet and superconductor geometry have fixed positions in the geometry component. There is a separation in distance between the magnet and the superconductor. This separation is referred to as the air gap which initially was set at 10 mm.

The model was imported on the XY plane to ensure that the axial direction of the magnet and superconductor are on the z-axis with the superconductor below the magnet. Figure 25 displays the coordinate system in the right bottom corner of the figure. The geometry was then added to a magnetostatic analysis system in ANSYS Multiphysics.

An additional plane was added to the bottom base of the magnet. It was defined as the polarisation plane and used to allocate direction to the magnetic field flowing from the magnet. Thus the direction of the magnetic field was set to be in the direction of negative z-axis with respect to the global coordinate system. Figure 25 shows the polarization plane on

the magnet with the red arrow pointing up in the positive z-direction with respect to the global coordinates.

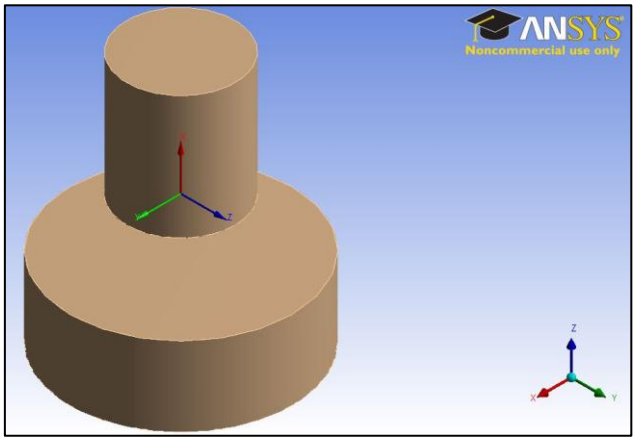

Figure 25: CAD model of the simulated permanent magnet at a levitation gap of 10 mm.

To evaluate the forces of the interactions of the magnetic field of the magnet with the superconductor it was necessary to add air elements to the simulation environment in the form of a cubic enclosure with side length 0.2 m (0.008 m^3). This enclosure represents air that envelops the magnet and superconductor.

For the magnet and superconductor material properties, two new materials were defined in the Engineering Data component of the magnetostatic analyses of the forces between the magnet and superconductor. Only magnetic properties which correspond with a magnetostatic analysis were defined for the permanent magnet and superconductor materials in the materials database of the Engineering Data component as air is defined by default in the Engineering Data component.

The only material properties that were defined and allocated to the elements are:

1) Yttrium barium copper oxide superconductor (YBCO) with:
    i) Isotropic Relative Permeability, $\mu_r = 0.001$
2) Neodymium magnet (NdFeB) with:
    i) Residual Induction, approximately $\boldsymbol{B_r} = 1.24\ T$
    ii) Coercive Force, approximately $\boldsymbol{H_c} = 860\ kA/m$
3) Air:
    i) Isotropic Relative Permeability, $\mu_r = 1$

In theory $\mu_r = 0$ for a superconductor sample below its critical temperature. ANSYS would not solve for $\mu_r = 0$ for a superconductor below T_c and for this reason $\mu_r = 0.001$ was defined

in the YBCO material database, for the simulation to have a relative permeability of nearly zero.

Although $\mu_r = 0.001$ was defined for the YBCO material, other magnetic properties were not defined for YBCO, because they are incompatible with the addition of relative permeability. In the ANSYS Mechanical platform the materials were allocated to the different geometries.

An environment was defined in which the magnetic flux generated by the magnet was measured. This was done by selecting the faces of the air enclosure and defining the six faces as the “magnetic flux parallel” region boundaries.

A mesh that was automatically generated by the ANSYS Mechanical code was used to solve the model. Use of the automatically generated default mesh was recommended by an expert on ANSYS solutions in personal communication (Mr Francis van Ravenswaay). The simulation was set to solve for one step of one second which was sufficient to gain a solution.

Solution information was gathered by adding “Directional force” plots which displayed the force summation over the magnet, superconductor and combination of the two. The latter summation was done to see whether the forces balanced out over the permanent magnet and YBCO superconductor.

Once the forces were determined at 10 mm the air gap was reduced by 1 mm, by manually editing the geometry. The simulation was then re-run and solved and the resulting forces were determined for the geometry with the updated air gap. These steps were repeated until the resulting force was determined between the magnet and superconductor at an air gap of 0 mm.

Figure 26 is a graph of the magnitude of the forces at given air gaps, which were determined in the simulation study, between a magnet and a superconductor below its T_c. The force on the magnet (line labelled “PM”) increases as the air gap decreases from 10 mm to 1 mm. It is also true for the reaction force on the superconductor (line labelled “YBCO”). The line labelled “SUM” is the sum of these forces at each air gap interval.

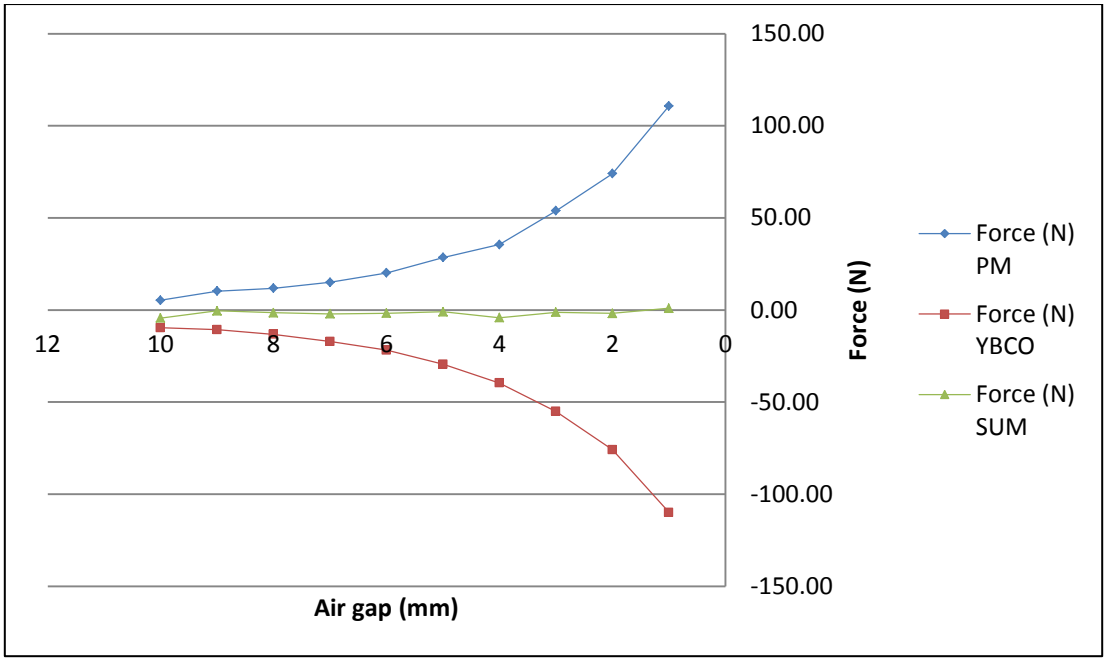

Figure 26: Graph for levitation forces acting on the superconductor, magnet and the sums of forces at each air gap interval obtained from simulations.

From Figure 26, at 10 mm the force on the superconductor should theoretically be 0 N, because for a pinned field ($\mu_r = 0$) the superconductor and magnet would be in equilibrium with the magnet levitating above the superconductor. However the superconductor, $\mu_r = 0.001$ was set in the simulation which is an approximated case of levitation and pinning.

Thus the action and reaction forces were not equal hence the sum of forces is not zero at each interval. For $\mu_r = 0$ (ideal case of levitation and pinning) the sum of forces is theoretically zero at each interval, which indicates stable levitation of the magnet above the superconductor.

The sum of forces was used as a measure of accuracy of the model, in which $\mu_r = 0.001$ was set, by comparing the sums of forces of the model with those of the ideal case of pinning ($\mu_r = 0$). It was found that the larger the difference between the sums of forces of the ideal case ($\mu_r = 0$) and approximated case ($\mu_r = 0.001$), the less accurate the model is. The resulting forces obtained for the approximated case are presented in Table 2 for the forces working on the permanent magnet and superconductor.

Table 2: Table for the forces determined in the simulation acting on the magnet and superconductor and the sums of forces at each air gap interval.

Position (mm)	10	9	8	7	6	5	4	3	2	1	0
Force (N) PM	5.30	10.25	11.75	15.04	20.10	28.46	35.49	53.84	74.04	110.81	4.19
Force (N) YBCO	-9.68	-10.71	-13.27	-17.15	-21.84	-29.46	-39.66	-55.08	-75.85	-109.91	-71.19
Force (N) SUM	-4.38	-0.46	-1.52	-2.11	-1.74	-1.00	-4.17	-1.24	-1.81	0.90	-67.00

As presented in Table 2, the sums of the forces at their specific air gaps do not deviate much from the ideal case ($\mu_r = 0$) where the sum of forces over each interval is zero. The largest deviance is 1.16 N at air gap 10 mm. The deviance in the sums of force are plotted in Figure 26 and labelled “Force Sum”.

Note that the forces at 0 mm are not plotted on the graph. The reason for this is that once the air gap is 0 mm the magnet and superconductor make contact creating conduction paths which defeats the purpose of levitation as suspension mechanism.

ANSYS also calculated action and reaction forces at 0 mm, which were smaller than the forces at 1 mm. This result is not accurate according to what was gathered in the literature survey because the forces are to increase as the air gap nears 0 as Chen *et al.* (1998) found during experimental tests.

3.3.4 Summary

The results obtained in the mathematical- and finite element studies for the forces acting between a superconductor and a permanent magnet differ in magnitude as presented in Figure 27. The forces obtained in the mathematical study (line labelled “Calculation”) have a maximum force of approximately 0 N compared to the approximate 110 N obtained in the finite element study (line labelled “Simulation”) at 1 mm air gap.

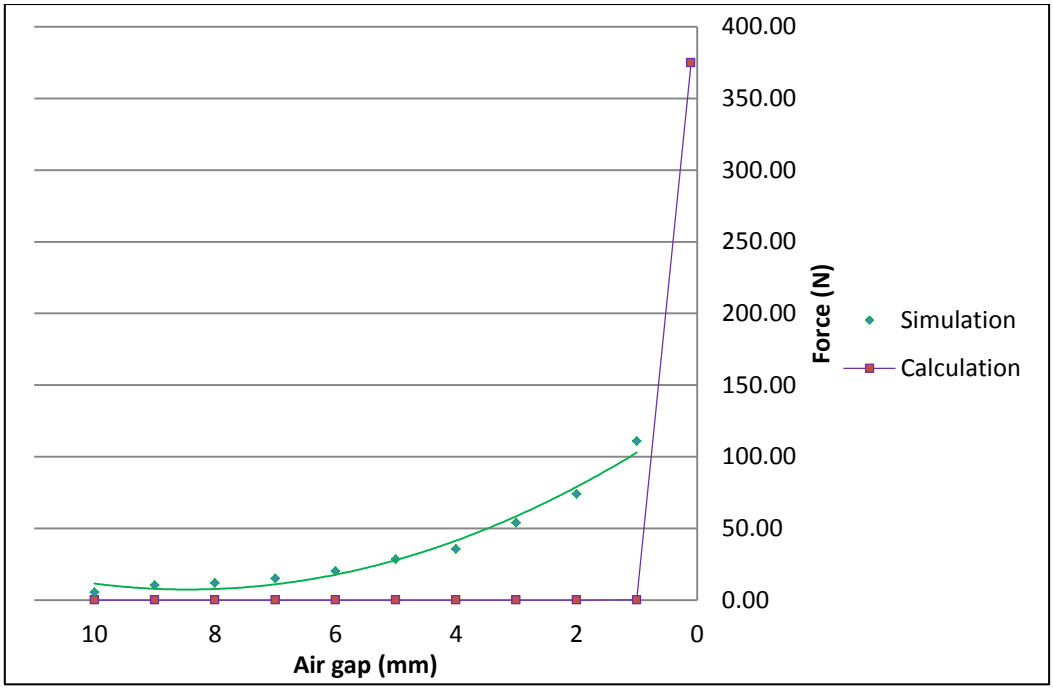

Figure 27: Graph for levitation forces measured in the mathematical- and finite element study.

The force magnitude of the finite element study decreases with an increase in air gap, whereas for the mathematical study it is constant 0 N. The discrepancies in magnitudes of the forces between a magnet and superconductor obtained in the mathematical- and finite element study is investigated in Chapter 4.2.

Chapter 4: Concept validation

To assess the calculated levitation force magnitudes for the electromagnetic- and superconducting suspension mechanism, experimental tests were carried out to measure said levitation forces and ultimately validate the magnetic suspension concept. The experimental procedures as well as the results obtained for the levitation force magnitudes, during these tests are covered under the following headings:

- Electromagnetic suspension
- Superconducting suspension

4.1 Electromagnetic suspension

4.1.1 Experimental study

To validate the use of an electromagnet for magnetic suspension of the inner vessel an electromagnet was built according to the specifications given in Chapter 3.1.1. It was connected to a power source of 220 V and 14.5 A (alternating current). An aluminium plate was then levitated above the electromagnet.

The magnetic levitation force between the plate and electromagnet was measured by placing weights on the aluminium plate until the weight of the weights overcame the levitation force. The electromagnet produced a levitation force that lifted approximately 2.24 kg. The corresponding levitation force is calculated at approximately 22 N which is far below the required 610 N to suspend the inner vessel. The force produced by the magnet is also far below the calculated force of 660 N, which the magnet was expected to produce.

4.1.2 Discussion

The weak force produced, is ascribed to the heat dissipation in the electromagnet as well as impurities in the aluminium plate. It is also believed that due to the coil having many air gaps between windings a uniform field could not be created inducing weaker eddy currents in the aluminium plate.

A power consumption of 3.19 kW was calculated for the electromagnet which produced a 22 N levitation force. To produce a lift force of 610 N approximately 28 electromagnets that produce a force of 22 N each, are required. This results in a power loss of approximately 90 kW for the sum total of electromagnets.

In the case of electromagnetic suspension as discussed in Chapter 3.3.1, 28 electromagnets require approximately 0.75 g/s to drive the electromagnets, while filling of the container takes place. If filling takes place for 2 minutes the required mass of hydrogen is approximately 0.09 kg L-H_2 to drive the electromagnets while the superconductors make the transition from the normal state to the superconducting state.

4.1.3 Conclusion and recommendations

It is the conclusion of this study that electromagnetic levitation must not be made use of as suspension mechanism for the inner vessel. This conclusion is based on the loss of hydrogen which is incurred to drive the electromagnet, while it is being used to levitate the inner vessel during L-H_2 filling.

It is recommended that another method is investigated to suspend the inner vessel within the outer vessel as superconducting levitation is initialized. A possible method is the use of an air bag which is positioned between the inner and outer vessel and attached to the outer vessel inner wall. While superconducting levitation is induced the air bag is inflated to position the inner vessel within the outer vessel at 10 mm air gap between the magnets and superconductors.

Once the superconductors have pinned the magnetic fields of the inner vessel the air bag is deflated and a vacuum in the outer vessel is drawn. The air bag then lies against the outer vessel wall and doesn't make contact with the inner vessel. Hence there is no conduction path. Figure 28 is a CAD model of an inflated air bag in the container concept.

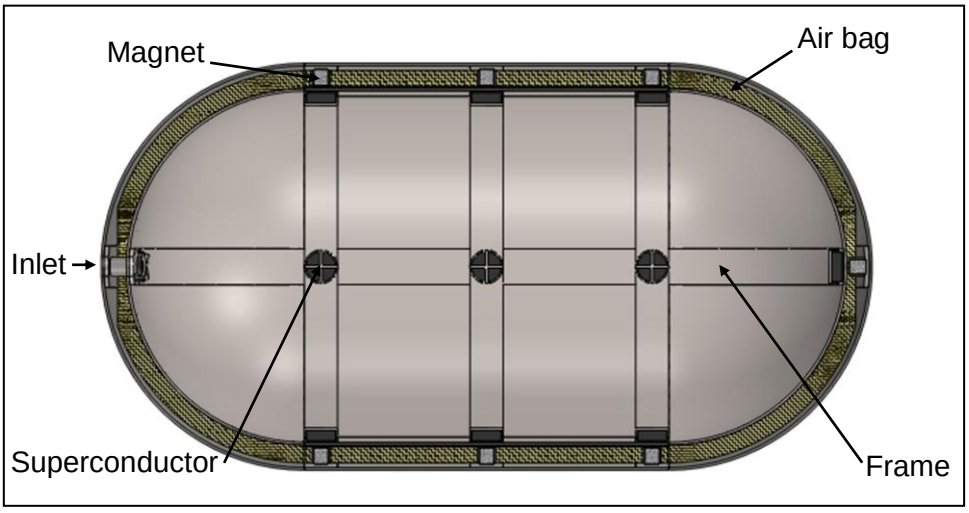

Figure 28: Top section view of a CAD model for the concept wherein an air bag is used to suspend the inner vessel while superconducting levitation is initiated.

An important factor for the air bag design is the material selection of the air bag as the bag must be able to withstand cryogenic temperatures when in contact with the inner vessel wall and in the possible chance of liquid hydrogen spillage on the bag. Another important factor is that the air bag must not become brittle due to the cold temperature it is exposed to.

During the experimental tests for the forces between a magnet and a superconductor a piece of the Dyneema braid was submerged in the liquid nitrogen for a short period of time and then an attempt was made to snap the braid by manually exerting a tensile force on the braid. The braid did not fail under the tensile force applied to it after exposure to liquid nitrogen temperature.

Based on the fact that the Dyneema did not fail under the tensile force and was very much flexible after coming into contact with the liquid nitrogen it is suggested that an air bag be woven from Dyneema braid. However research should be done on Dyneema braid and other possible materials for use in air bag design.

Another design aspect to consider for the use of an air bag is the joining of the bag to the outer vessel inner wall. This may be achieved with an epoxy resin. However the choice of epoxy must be investigated to determine the temperatures it can function at, as it may be exposed to the liquid hydrogen stored in the inner vessel.

4.2 Superconducting suspension

4.2.1 Experimental study

To investigate the difference in results of the mathematical study and finite element study and validate superconducting levitation as suspension mechanism for the concept, the forces between one permanent magnet and superconductor were measured experimentally at air gaps ranging from 0 mm to 10 mm.

Data provided by suppliers for which the design calculations are based on was used in these experiments. The results of these experiments are compared to the results obtained in the mathematical and finite element studies.

Although the concept of this study is for use in cryogenic containers for the storage of L-H_2, L-N_2 was used in all experiments to achieve the superconducting state in the YBCO sample because the temperature of L-N_2 (77 K or -196.15 °C) is sufficient to achieve magnetic field pinning in the superconductor.

L-H_2 causes better pinning properties and stronger levitation forces at its lower temperature, based on the findings of Gruss *et al*., (2001) that fluids with lower temperatures induce better pinning properties resulting in more flux being pinned in a superconductor, mentioned in the literature study. L-N_2 does not present a fire hazard and for this reason it is preferred above L-H_2 for use in the experimental tests.

Again it is mentioned that a single grain melt textured YBCO sample was used due to its excellent flux trapping capabilities as discussed in the literature study (Chen, *et al*., 1998). NdFeB magnets were used for the experimental tests due to the strong magnetic forces and greater stiffness the magnets deliver which was also discussed in the literature study (de Andrade Jr., *et al*., 2003).

A test bench was built from 16 mm thick super wood. Super wood was used to minimize any magnetic effects on the magnet and superconductor during force measurement. A perspex holder was built to keep the magnet in horizontal position above the superconductor. Two perspex guides were built to guide the magnet holder in a vertical direction to ensure that the magnet face would stay parallel with the superconductor face. Figure 29 is a schematic of the experimental setup.

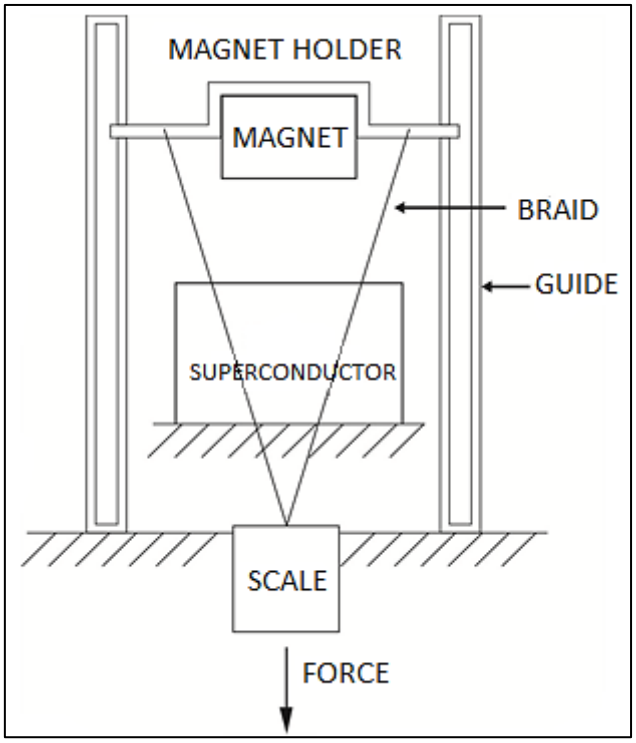

Figure 29: Schematic of the experimental setup. For simplicity reasons the holder in which the superconductor is cooled is not displayed in this schematic.

Woven Dyneema braid (elongation < 3.5 %) was attached to the magnet holder at one end and at the other end to an electronic scale (maximum weight limit of 40 kg), which was used to measure the forces between the magnet and superconductor.

The superconductor was placed in an aluminium holder in which liquid nitrogen was poured. A 10 mm thick perspex beam was placed on top of the superconductor while the magnet was placed on the perspex beam.

To ensure temperature equilibrium between the superconductor and the holder, the holder was filled with liquid nitrogen nearly covering the superconductor. The superconductor was left in the holder for ample time to cool and achieve the strongest possible trapped field and levitation force at liquid nitrogen temperature (77 K or -196.15 °C).

Once the liquid nitrogen stopped boiling around the superconductor and in the container, the superconductor and container had reached equilibrium. This was the sign that flux trapping had finished taking place while field cooling the superconductor. Figure 30 is a schematic of the magnet (labelled PM) at initial condition where the air gap is 10 mm and $\boldsymbol{F} = 0\ N$ between the superconductor (below T_c) and magnet. The flux lines are pinned in the superconductor.

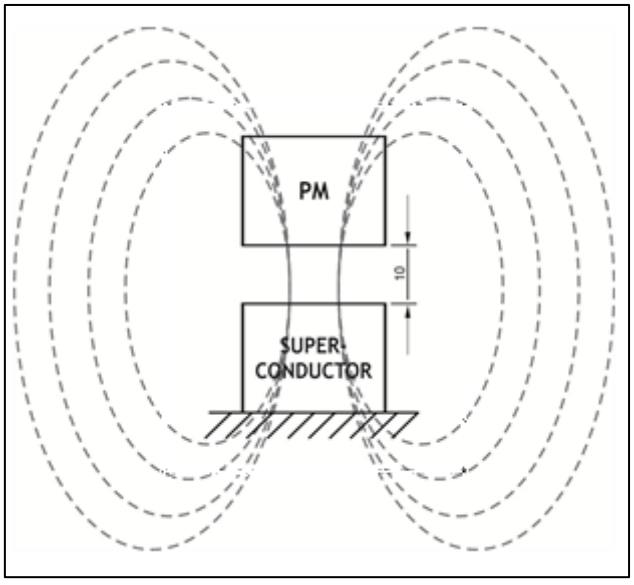

Figure 30: Schematic of the field lines of the neodymium magnet pinning in the YBCO superconductor at an air gap of 10 mm.

The magnetic field was pinned in the superconductor with the magnet stably levitating above the YBCO sample at 10 mm. Figure 31 is a picture of a magnet in the magnet holder levitating above the superconductor. Once flux trapping had taken place, the measurements of reaction force on the magnet were taken.

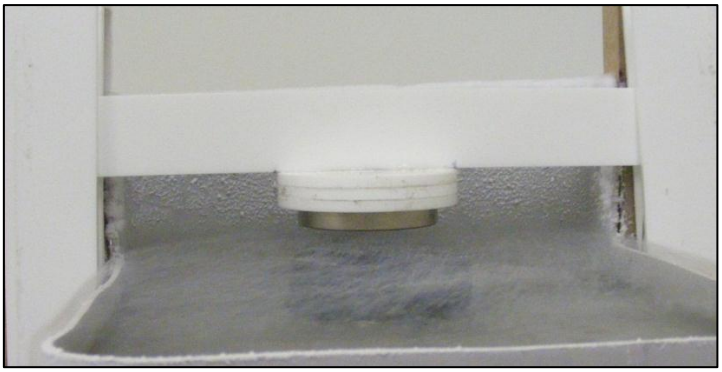

Figure 31: Photo of the neodymium magnet in its holder while pinned and levitating above the YBCO superconductor which is in the superconducting state.

By manually exerting a downward force on the scale the magnet was displaced from an air gap of 10 mm to an air gap of 0 mm. This downward force in turn caused a reaction force on the magnet which was measured with the scale.

The first measurement was taken at 9 mm because the magnet was in equilibrium at 10 mm resulting in zero reaction force acting on the magnet. Reaction forces on the magnet were measured three times at each interval of air gap displacement. Measurements were taken at increments of 1 mm until the magnet made contact with the superconductor.

The averages of the three force measurements at each air gap were calculated and are presented in Table 3 for two sets of experiments as this experiment was conducted twice. However, there are small differences between the magnitudes of the averages of forces for Test 1 and Test 2.

These differences are ascribed to the superconductor not being in thermal equilibrium with the aluminium holder. For Test 2 the superconductor was cooled for a longer period of time before measurements were taken which led to a better thermal equilibrium and ultimately better flux trapping and stronger levitation forces than that which was achieved in Test 1.

Table 3: Table for the levitation forces determined between the magnet and superconductor in the experimental study for Test 1 and Test 2.

Position (mm)	10	9	8	7	6	5	4	3	2	1	0
Force (N) Experiment 1	0.00	2.65	3.11	3.43	3.96	6.31	9.81	13.54	16.61	21.71	23.25
Force (N) Experiment 2	0.00	1.24	4.68	5.72	7.10	9.65	13.60	15.30	17.89	24.98	29.69

The maximum force that was measured at 1 mm is approximately 25 N for Test 2 at air gap position 1 mm. At 0 mm air gap the magnet and superconductor made contact which then

created a thermal conduction path defeating the purpose of superconducting levitation as suspension mechanism. For this reason Figure 32 presents the graphs for the average forces presented only from 1 mm to 10 mm air gap. At 10 mm the magnet levitated above the superconductor in equilibrium.

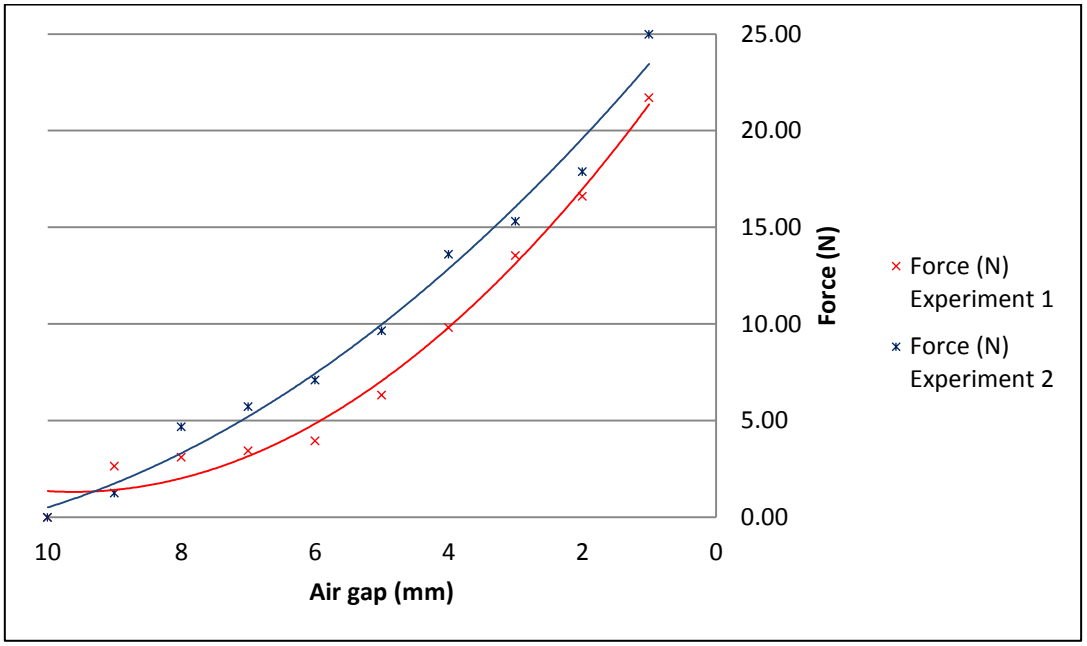

Figure 32: Graph of the two tests conducted for the forces measured between a magnet and superconductor at specific air gap increments.

4.2.2 Discussion

The experimental results are compared to the results obtained during the finite element- and mathematical studies. Figure 33 is a graph of levitation force as a function of air gap, for the forces measured experimentally and determined by calculation and simulation, between a 22 mm diameter neodymium magnet and a 45 mm diameter YBCO superconductor.

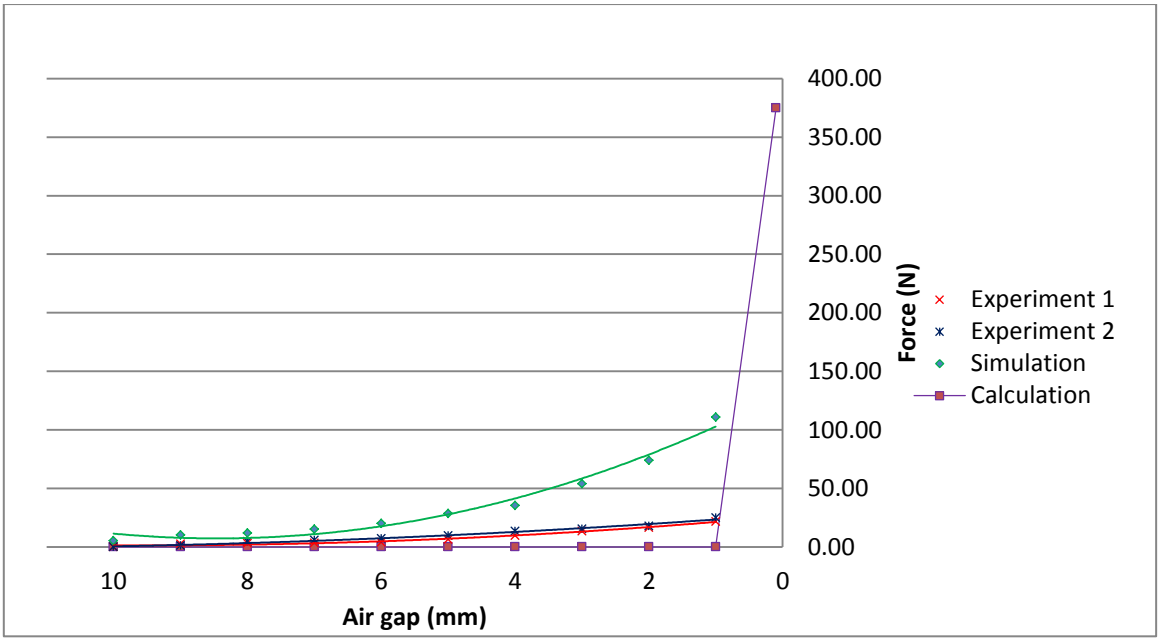

Figure 33: Graph of levitation force as a function of air gap, measured experimentally and determined by calculation and simulation, between a neodymium magnet and a superconductor.

The form of the graph of levitation forces calculated with the equation derived by Fedda *et al.*, (2007) (labelled "Calculation") is a flat line with a spike as it nears 0 mm in Figure 33. From the literature survey, graphs of levitation force versus air gap were found to have increases in levitation force with decreases in the air gap as the air gap neared 0 mm (Fuchs, *et al*., 2005). The forms of these graphs of Fuchs, *et al.* (2005) were equal to the forms of graphs for quadratic equations.

It is believed that the discrepancy in the graph form is due to the force being calculated in the limit $\lim_{a\to 0} F$ (see Equation 17). Equation 17 does not consider the outer diameter of the superconductor in the formula. Hence the formula becomes an infinite superconducting plane and is no longer a disk. This means that the magnetic dipole is infinitely smaller than the superconductor.

Although Fedda *et al.* (2007) found that for small magnets Equation 17 delivered results matching those of experimental tests conducted by Ma *et al.* (2001), it is concluded that this model is not valid for use to determine the forces between the magnets and superconductors of this study. It is believed that the magnets of this study are too large in comparison to the size of the superconductors.

The results obtained in the FE studies and those of the experiments, for the levitation forces between the magnet and superconductor did not match. The levitation forces measured in

the experiments were much weaker than the magnitudes of forces obtained in the calculations and FE studies as presented in Figure 33.

An investigation into this discrepancy proved that the magnet had weaker magnetic properties than specified by the manufacturer. The residual induction was given as $\boldsymbol{B_r} = 1.2\ T$, but it was measured with a magnetometer to be $\boldsymbol{B_r} = 0.62\ T$.

The coercive force was given as $\boldsymbol{H_c} = 860\ kA/m$ and could not be measured due to instrumentation shortcomings. However, using data sheets given by the supplier of a range NdFeB magnets and the measured $\mathbf{B_r}$ value, it was calculated by extrapolation that $\boldsymbol{H_c} = 440.4\ kA/m$.

The new magnetic properties were then introduced into the FE simulation which generated new results for the forces between the magnet and superconductor. The forces of the superconductor and permanent magnet as well as the sum of forces are plotted in Figure 34 as a function of air gap.

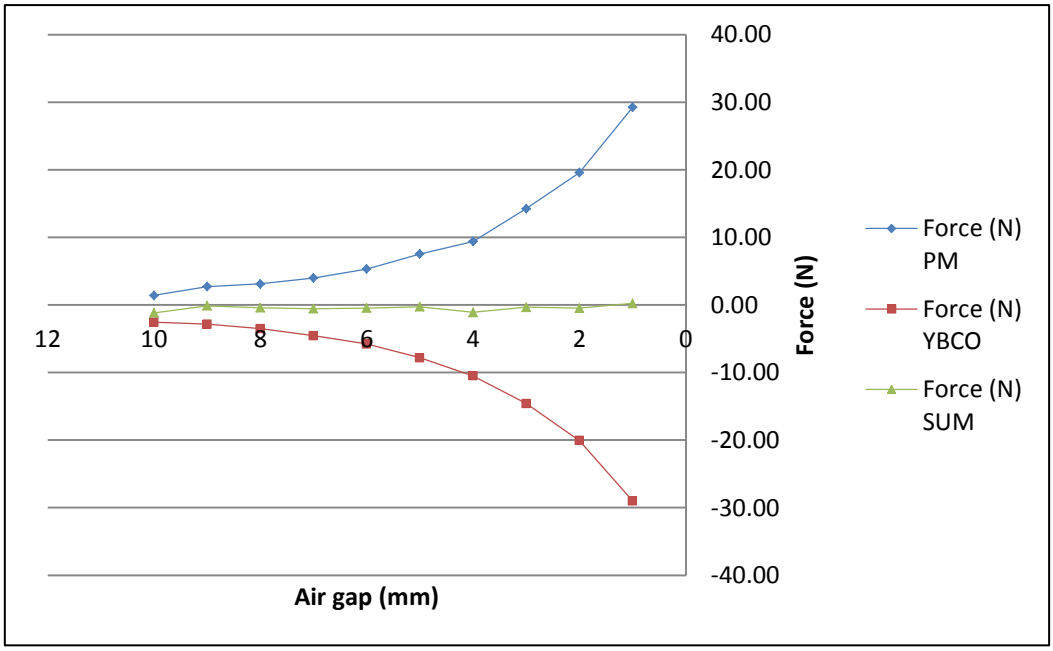

Figure 34: The graph for levitation forces acting on the superconductor, magnet and the sums of forces as a function of air gap interval, obtained from simulations for the measured magnetic properties of the magnet.

Table 4 lists the new results obtained in the finite element study for forces between a magnet and a superconductor using the measured $\mathbf{B_r}$ and calculated $\mathbf{H_c}$ values of the permanent magnet in the simulations.

Table 4: Table for the forces determined in the simulation acting on the magnet and superconductor and the sums of forces as a function of air gap position for the measured magnetic properties of the magnet.

Position (mm)	10	9	8	7	6	5	4	3	2	1	0
Force (N) PM	1.41	2.72	3.12	3.99	5.33	7.54	9.40	14.26	19.58	29.26	1.12
Force (N) YBCO	-2.57	-2.84	-3.52	-4.55	-5.79	-7.81	-10.51	-14.59	-20.06	-29.02	-18.86
Force (N) SUM	-1.16	-0.12	-0.41	-0.56	-0.46	-0.27	-1.11	-0.33	-0.48	0.24	-17.75

The results obtained in the finite element studies in which the measured magnetic properties of the magnets were used, are compared to the test results obtained during experimental studies for the forces between the magnet and superconductor. The values for the levitation force on the magnet are now in good agreement with those of the experimental tests. These forces are plotted as a function of air gap in Figure 35.

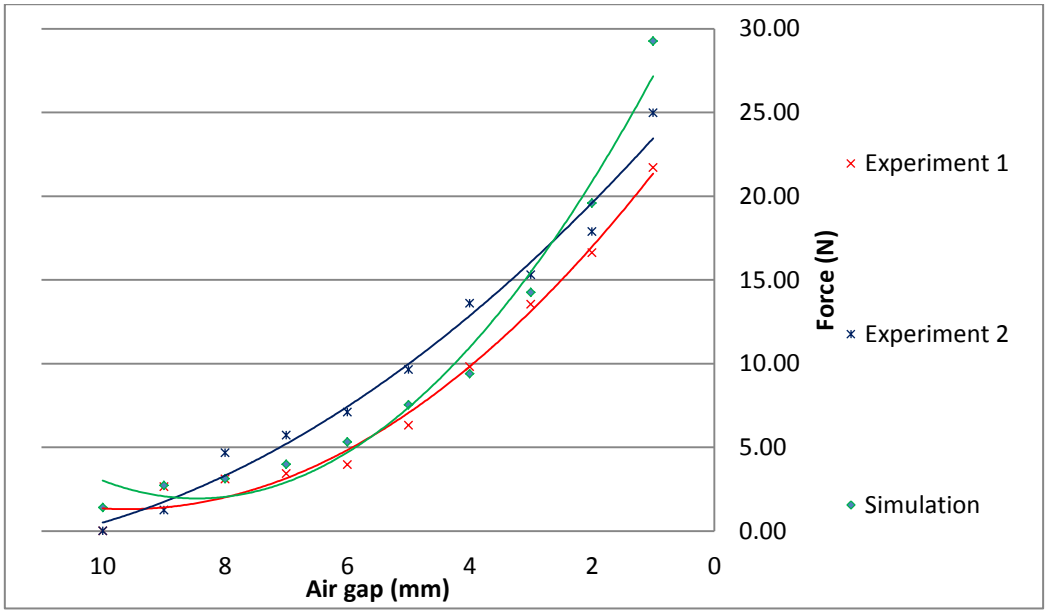

Figure 35: Graph of levitation forces between the superconductor and magnet as a function of air gap interval obtained during experiments and simulations for the measured magnetic properties of the magnet.

The discrepancies between the experimental results and simulation results are ascribed to the temperatures at which the superconductor was while measurements were taken during experiments. It was mentioned in the literature survey that field pinning is reliant on the superconductor temperature. The colder the temperature of the superconductor is, the

better the pinning properties of the superconductor are. Therefore stronger relationship between the results for the experimental tests should be possible at colder temperatures.

To ensure that the superconductor temperature stayed below its T_c, liquid nitrogen was added to the superconductor holder between measurements. The addition of L-N_2 ensured that the superconductor stayed in the superconducting state ($\mu_r = 0$) throughout experimental tests.

For the simulations magnetic field penetrated the superconductor but it was not pinned, because $\mu_r = 0.001$. Although ANSYS couldn't solve for $\mu_r = 0$, the results generated give a good indication of the force between a magnet and a superconductor because the results of levitation force gathered from the simulations are near to those in magnitude of the physical experiments.

Based on these findings, it is concluded that ANSYS may be used in future studies to determine approximate levitation forces between a magnet and a superconductor if the correct magnetic properties and data are provided by the supplier. The experimental results validated the results obtained during finite element modelling and simulations for force between a magnet and superconductor in the superconducting state.

4.2.3 Conclusion and recommendations

The magnetic suspension concept presented and discussed in Chapter 3 for suspension by means of superconducting levitation makes use of three permanent magnet-and-superconductor pairs to deliver the required superconducting levitation force to suspend the inner vessel within the outer vessel.

However the three magnet-and-superconductor pairs produced a maximum force of 25 N per magnet-and-superconductor pair at 1 mm air gap (Test 2). The total sum force of these three magnet-and-superconductor pairs at 1 mm is 75 N which is less than the 610 N force required to levitate the inner vessel. It is calculated that approximately 24 pairs of these magnet-and-superconductor pairs are required to produce the levitation force of 610 N at an air gap of 1 mm.

However a levitation gap of 1 mm is not possible as the inner vessel wall and inner vessel support rings have a combined thickness of 6 mm and the magnet caps have a thickness of 1 mm. As mentioned there is only a 3 mm gap between the inner vessel wall and magnet support rings (see Figure 23). At 6 mm levitation gap the inner vessel rests on the magnet caps creating a conduction path which is unwanted. Therefore the inner vessel may not

move to a position of less than 7 mm levitation gap between the magnet and superconductor.

The largest levitation force that was obtained experimentally at 7 mm levitation gap is approximately 5.7 N during Test 2. To produce a levitation force of 610 N approximately 107 magnet-and-superconductor pairs are required. The 107 magnet-and-superconductor pairs in turn require the addition of more support rings in which the superconductors can be mounted. The addition of more support rings increases the inner vessel weight giving rise to the requirement of more magnet-and-superconductor pairs.

It is the conclusion of this study that for the current design, the forces between the magnets and superconductors are not able to achieve the required forces for magnetic suspension of the inner vessel by means of superconducting levitation at a levitation gap of 7 mm due to the shortcomings of the obtained magnet and superconductor materials. This conclusion is based on the findings in the latest simulation results and the results obtained experimentally for the forces between a magnet and superconductor.

However it is believed that the use of forces generated between NdFeB magnets and bulk superconductors is feasible for inner vessel suspension in cryogenic pressure vessels if the magnitudes of these forces are improved.

Recommended methods to improve levitation forces of the superconductor and specifically the forces at 7 mm air gap for the suspension concept of this design, include the use of superconductors that have been doped with silver and zinc or that have undergone neutron irradiation which was discussed in the literature study and to use stronger NdFeB magnets such as N55 grade neodymium magnets (Fuchs, *et al*., 2005; Gruss, *et al*., 2001; Fuchs, *et al*., 2003).

It is also suggested that the inner vessel support frame be manufactured from a different material such as Aluminium 5083 which has a density of 2660 kg/m^3 and is much less dense than Ti-5Al-2.5Sn which has a density of 4480 kg/m^3. This will lower the frame mass and ultimately reduce required levitation forces. By lowering the internal storage pressure the internal vessel wall thickness may also be reduced, lowering the mass of the inner vessel and also producing a larger gap between the inner vessel wall and magnet caps.

As discussed in the preceding paragraphs it is clear that the purpose of the study was met as a concept for the storage of liquid hydrogen was proposed and validated on the basis of results obtained experimentally and by finite element analyses for the magnitude of levitation forces between an YBCO disk and NdFeB magnet. However it is believed that the proposed

recommendations should be carried out if the concept were to be investigated further for possible future implementation.

Chapter 5: Bibliography

© Volkswagen, 2012. *Golf Range.* [Online] Available

at: http://www.vw.co.za/en/models/golf/trimlevel_overview.html
[Accessed 25 October 2012].

Aceves, S., Berry, G. & Weisberg, A. H., 2004. *Lightweight cryogenic-compatible pressure vessels for vehicular fuel storage.* United States of America, Patent No. 6708502.

Aceves, S. M., Espinosa-Loza, F., Ledesma-Orozco, E., Ross, T.O., Weisberg, A.H., Brunner, T.C., Kircher, O., 2009. High-density automotive hydrogen storage with cryogenic capable pressure vessels. *International journal of hydrogen energy,* December, Volume 35, pp. 1219-1226.

Askeland, D. R. & Phulé, P. P., 2003. *The Science and Engineering of Materials.* Fourth Edition ed. California: Brooks/Cole - Thomson Learning.

Bleuler, H. Cole, M., Keogh, P., Larsonneur, R., Maslen, E., Nordman, R., Okada, Y., Schweitzer, G., Traxler, A., 2009. *Magnetic Bearings.* s.l.:Springer.

Chen, I.-G., Hdu, J.-C. & Wu, M.-K., 2001. Calculation of Magnetic Levitation/Suspension Force of Single Grained Y-Ba-Cu-O Superconductors. *IEEE Transactions on Applied Superconductivity,* 11(1), pp. 1745-1748.

Chen, I.-G., Hsu, J.-C., Janm, G., Kuo, C.-C., Liu, H-J, Wu, M.K., 1998. Magnetic levitation force of single grained YBCO materials. *Chinese journal of physics,* April, 36(2), pp. 420-427.

Chen, I.-G., You, L.-C., Hsu, S.-H. & Hsieh, P.-C., 2007. *How superconducting levitation works,* s.l.: s.n.

Collings, E. W., 1994. *Materials Properties Handbook: Titanium Alloys.* 1 ed. s.l.:ASM International.

de Andrade Jr., R., Cardoso, J. A. A. S., dos Santos, G. C., de Cicco, L. B., Fernandes, A. F. G., Rosario, M. A. Pd., Neves, M. A., de Souza, A. P., Ripper, A., da Costa, G. C., Nicolsky, R., Stephan, R. M., 2003. Performance of Nd-Fe-B and ferrite magnets in superconducting linear bearings with bulk YBCO. *IEEE transactions on applied superconductivity,* June, 13(2), pp. 2271-2274.

De Bruyn Ouboter, R., 1997. Heike Kamerlingh Onnes's Discovery of Superconductivity. *Scientific American,* March.pp. 98-103.

Energy, U. D. o. E. -. E. E. a. R., 2011. *Fuel Cell Technologies Program – Education.* [Online]
Available at: http://www1.eere.energy.gov/hydrogenandfuelcells/education/printable_versions/basics_storage.html
[Accessed 2 July 2012].

Fedda, A. Y., Alqadi, M. K., Al-Khateeb, H. M. & Ayoub, N. Y., 2007. The interaction force between a permanent magnet and a superconducting ring. *IEEE Transaction on applied superconductivity,* September, 17(3), pp. 3814-3818.

Fossheim, K. & Sudboe, A., 2004. *Superconductivity: Physics and Applications.* s.l.:Wiley and Sons Inc.

Fuchs, G., Krabbes, G., Muller, K.-H., Verges, P., Schultz, L., Gonzalez-Arrabal, R., Eisterer, M., Weber, H. W., 2003. High magnetic fields in superconducting permanent magnets. *Journal of Low Temperature Physics,* October, Volume 133, pp. 159-179.

Fuchs, G., Krabbes, G., Verges, P., Canders, E.-R., May, H., 2005. *Superconducting magnetic bearings for rotatin*g machines. Dresden, s.n., pp. 115-119.

Gruss, S., Fuchs, G., Krabbes, G., Verges, P., Schatzle, P., Muller, K.-H., Fink, J., Schulta, L., 2001. Trapped fields beyond 14 Tesla in bulk YBa2Cu3O7-δ. *Applied superconductivity,* March, 11(1), pp. 3720-3723.

Hauser, A., 1997. Calculation of superconducting magnetic bearings using a commercial FE-program (ANSYS). *IEEE Transactions on magnetics,* March, 33(2), pp. 1572-1575.

Iwasa, Y., 2009. *Case Studies in Superconducting Magnets: Design and Operational Issues.* 2nd ed. s.l.:Springer.

Jha, A. R., 1988. *Superconductor Technology: Applications to Microwave, Electro-Optics, Electrical Machines, and Propulsion Systems.* 1st ed. s.l.:John Wiley & Sons Inc.

Lewin, W., 2002. *8.02 Spring 2002 Lecture 19: Vacation Special,* s.l.: s.n.

Ma, K. B., Postrekhin, Y., Ye, H. & Chu, W.-K., 2001. Magnetic Interaction Force between High-Tc Superconductor-Ring and Magnet. *IEEE Transaction on applied superconductivity,* 11(1), pp. 1665-1668.

MatWeb, LLC, 2012. *MatWeb Material Property Data.* [Online] Available at: http://www.matweb.com/search/DataSheet.aspx?MatGUID=e2147b8f727343b0b0d51efe02

a6127e&ckck=1
[Accessed 3 December 2012].

Mérida, W. & Dicken, C., 2007. Measured effects of filling time and initial mass on the temperature distribution within a hydrogen cylinder during refuelling. *Journal of Power Sources,* January, Volume 165, pp. 324-336.

Murai, T., 1987. *Cryogenic container.* United States of America, Patent No. 4680935.

NdFeB Specialists E-Magnets UK Limited, 2011. [Online]
Available at: http://www.ndfeb-info.com/neodymium_grades.aspx

Neves, M. A., da Costa, G.C., Pereira, A.S., de Andrade Jr. R., Nicolsky, R, 2002. Mean field Jc Estimation for levitation device simulations in the bean model using permanent magnets and YBCO superconducting blocks. *Brazilian journal of physics,* September, 32(3), pp. 759-762.

NPL Management Limited, 2012. *National Physical Laboratory.* [Online]
Available at: http://www.npl.co.uk/reference/faqs/what-do-high-vacuum-and-low-vacuum-mean-(faq-pressure)
[Accessed 19 November 2012].

Perini, E., Giunchi, G., Geri, M. & Morandi, A., 2009. Experimental and Numerical Ivestigation of the Levitation Force Between Bulk Permanent Magnet and MgB2 Disk. *IEEE Transactions on Applied Superconductivity,* 19(3), pp. 2124-2128.

Clarke, R., 2011. *The force produced by a magnetic field.* [Online]
Available at: http://info.ee.surrey.ac.uk/Workshop/advice/coils/force.html
[Accessed October 2011].

Ramachandran, R. & Menon, R. K., 1998. An overview of industrial uses of hydrogen. *International Journal of Hydrogen Energy,* 23(7), pp. 593-598.

Reed, R. P. & Golda, M., 1997. Cryogenic composite supports: a review of strap and strut properties. *Cryogenics,* Volume 37, pp. 233-250.

Sable Magnetics, 2011. [Online] Available at: http://www.sabels.com/

Sakintuna, B., Lamari-Darkrim, F. & Hirscher, M., 2007. Metal hydride materials for solid hydrogen storage: A review. *International Journal of Hydrogen Energy,* January, Volume 32, pp. 1121-1140.

Schönhuber, P. & Moon, F. C., 1994. Levitation forces, stiffness and force-creep in YBCO high-Tc superconducting thin films. *Applied superconductivity,* 2(7/8), pp. 523-534.

Silver, D. M. & Dehaas, N., 1985. *Cryogenic tank support system.* United States of America, Patent No. 4496073.

Tsuchimoto, M., 2001. Shielding current model and frozen field model in analysis of magnetic force between a bulk HTS and a magnet. *Journal of Materials Processing Technology,* Issue 108, pp. 188-192.

van Vuuren, D. S., Hietkamp, S. & Benson, J., 2009. *Cryogenic Compressed Hydrogen Storage.* Somerset West, s.n., pp. 1-16.

Winter, C., 2009. Hydrogen energy - Abundant, efficient, clean: A debate over the energy-system-of-change. *International Journal of Hydrogen Energy,* Volume 34, pp. S1-S52.

Appendix A: Cryogenic supports

Reed and Golda (1997) found that E- and S-glass fibres had lower thermal conductivities at approximately 25 K (-248.15°C) than other fibre types, whereas carbon fibre composites had the highest thermal conductivity at 25 K.

Alumina fibres have a thermal conductivity between that of glass and carbon fibres at 4 K. Here follows some thermal conductivity values of some fibre materials at a temperature of 4K (Reed & Golda, 1997):

- Carbon fibres, 0.03 W/mK.
- Alumina fibres, 0.05 W/mK.
- E- and S-glass fibres, 0.10 W/mK.

The magnitude of the thermal conductivity of carbon fibre composites depends on the percentage of graphite fibres found in the carbon fibre composite. The more graphite fibres in a composite, the higher the Young's modulus and thermal conductivity are. It was found that at temperatures below 25 K, all carbon fibre types have more or less equal conductivities which are lower than that of glass- and alumina fibres (Reed & Golda, 1997).

Calculations of heat transfer and the effects thereof were carried out for support straps produced from carbon fibre with length, width and thickness of 70 mm, 30 mm and 2 mm respectively. Calculations for the heat transfer through E-glass support tubes were also carried out. The tube length is 70 mm and the minimum wall thickness of the tube is 2 mm. Thermal conductivities given by Reed and Golda (1997) were used. EES code for these calculations is given:

```
"!Duplicate loop in which heat loss through strap is calculated"

duplicate i=1,1

    q_x_flux[i] = - k[i] * (T_2[i] - T_1[i]) / L[i]      "Heat flux"

    k[i] = 0.03 [W/mK]                                   "Heat constant of carbon fibre straps"

    T_2[i] = 20 [K]                                      "Liquid hydrogen temperature"

    T_1[i] = 300 [K]                                     "Ambient temperature"

    L[i] = 0.07 [m]                                      "Length of part"

    A[i] = T[i] * W[i]                                   "Cross sectional area of strap"

    W[i] = 30 / 1000                                     "Width of strap"
```

```
T[i] = 2 / 1000                          "Thickness of strap"
h_fg[i] = 446 * 1000                     "Heat value for hydrogen"
q_x_heatloss[i] = A[i] * q_x_flux[i]     "Heat flow for one carbon strap"
q_x_heatloss_6[i] = q_x_heatloss[i] * 6  "Heat flow for six carbon straps"
m_dot[i] = q_x_heatloss[i] / h_fg[i]     "Mass loss of H2 per second per strap"
m_dot_24[i] = m_dot[i] * 24 * 3600       "Mass loss of H2 per day per strap"
m_dot_24h6[i] = m_dot_24[i] * 6          "Mass loss of H2 per day for six straps"
end
"!Duplicate loop in which heat loss through tube is calculated"
duplicate i=2,2
q_x_flux[i] = -k[i] * (T_2[i] - T_1[i]) / L[i]   "Heat flux"
k[i] = 16 * 0.24 / 73 + 0.06             "Heat constant of E-glass tube"
T_2[i] = 20                              "Liquid hydrogen temperature"
T_1[i] = 300                             "Ambient temperature"
L[i] = 0.07                              "Length of part"
A[i] = pi*(T[i])^2                       "Cross sectional area of tube"
r_i[i] = 0.013                           "Inner diameter of tube wall"
T[i] = r_o[i] - r_i[i]                   "Tube wall thickness"
r_o[i] = 0.001 +  r_i[i]                 "Outer diameter of tube wall"
h_fg[i] = 446 * 1000                     "Heat value for hydrogen"
q_x_heatloss[i] = A[i] * q_x_flux[i]     "Heat loss for one E-glass strut"
q_x_heatloss_6[i] = q_x_heatloss[i] * 6  "Heat loss for six E-glass struts"
m_dot[i] = q_x_heatloss[i] / h_fg[i]     "Mass loss of H2 per second per tube"
m_dot_24[i] = m_dot[i] * 24 * 3600       "Mass loss of H2 per day per tube"
m_dot_24h6[i] = m_dot_24[i] * 6          "Mass loss of H2 per day for six tubes"
end
```

Table 5 lists the results obtained solving the EES code given for determination of heat flow through the carbon and E-glass supports. The heat addition to hydrogen through the straps, as well as the loss of hydrogen due to boil-off, is given for one strap and six straps in row one. These values are also given for one tube and six tubes in row 2. The flux value shows the value of heat conducted through these supports over the support cross-sectional area.

Table 5: Results listed for calculations of heat flow through straps and tubes and hydrogen boil off due to heat flow through supports.

Sort	1 $\dot{m}_i$ [kg/s]	2 $\dot{m}_{24,i}$ [kg/s]	3 $\dot{m}_{24h6,i}$ [kg/s]	4 $q_{x,flux,i}$ [W/m^2]	5 $q_{x,heatflow,i}$	6 $q_{x,heatflow,6,i}$
[1]	1.614E-08	0.001395	0.008369	120	0.0072	0.0432
[2]	3.173E-09	0.0002741	0.001645	450.4	0.001415	0.00849

Appendix B: Hydrogen vessel calculations

The EES code used to calculate the required mass of hydrogen and required container size for storage of liquid hydrogen is presented below. The magnet size to produce levitation forces to suspend an inner vessel filled with L-H_2 within an outer vessel is also given in the code.

```
E_specific =  119930000 [J/kg]                "Specific energy"
rho_H2 = Density(Hydrogen,T=20,x=0)           "Liquid hydrogen density"
m_H2 =  E / E_specific                        "Hydrogen mass"
V_H2 = m_H2 / rho_H2                          "Hydrogen volume"
"!Container properties"
V_H2 = pi * r^2 * l + 4 * pi * r^3 / 3        "Inner radius calculated"
t = 0.004[m]                                  "Vessel Wall Thickness"
l = 0.55                                      "Cylinder length"
L_tot = 2 * r +l + 2 * t                      "Total length of the inner vessel"
m_container = (pi*(r+t)^2*l+4*pi*(r+t)^3 / 3 - V_H2 ) * rho_container "Mass container"
V_container = (pi*(r+t)^2*l+4*pi*(r+t)^3 / 3) "Container volume"
rho_container =  4480 [kg/m^3]                "Density of Ti-5Al-2.5Sn ELI"
sigma_u = 775 [MPa]                           "Ult. tensile strength Ti-5Al-2.5Sn ELI"
sigma_y =  720 [MPa]                          "Ult. yield strength of Ti-5Al-2.5Sn ELI"
P = 10 [MPa]                                  "Internal pressure of vessel"
sigma_1 = P * r / t                           "Stress"
sigma_2 = P * r / (2 * t)                     "Stress"
sigma_3 = P * r / (2 * t)                     "Stress"
SF = sigma_y / sigma_1                        "Safety factor"
m_total = m_container + m_H2 + m_support + m_sc "Mass of container and L-H2"
m_support = 13                                "Mass of support frame"
m_sc =2.5                                     "Mass of superconductor"
g = 9.81 [m/s^2]                              "Gravity constant"
```

```
F_total = m_total * g                          "Weight of filled container under gravity"
"!Permanent magnet"
F_total = B_pm^2 * A_pmbig / (2 * mu_0)        "Area of permanent magnet calculated"
B_pm = 1.24[T]                                 "Inductance"
A_pmbig = pi*r_pmbig^2                         "Radius of large PM calculated"
d_pmbig = r_pmbig * 2                          "Diameter of large PM calculated"
F_pm = F_total/3                               "Force of one smaller PM"
F_pm = B_pm^2 * A_pm / (2 * mu_0)              "Area of one permanent magnet"
A_pm = pi*r_pm^2                               "Radius of large PM calculated"
d_pm = r_pm*2                                  "Diameter of large PM calculated"
m_pm = F_pm / 9.81                             "Mass lifted by smaller PM"
mu_0 = 4 * pi / 10000000                       "Permeability of free space"
"!Electromagnet"
F_em = F_pm                                    "Electromagnet force"
F_em = (N*I)^2 * mu_0 * A_em/(2*L_em^2)        "Area of electromagnet"
N = 500 [turns]                                "Windings"
L_em = 0.015 [m]                               "Electromagnet length"
I = 14 [A]                                     "Current"
A_em = pi * r_em^2                             "Radius of electromagnet calculated"
d_em = r_em * 2                                "Diameter of electromagnet calculated"
Power_em = 90000 [W]                           "Power required for electromagnets"
E_em = Duration_sec_em * Power_em              "Energy required for electromagnets"
Duration_sec_em = 120                          "Electromagnet running time"
m_H2_em =  E_em / E_specific                   "Hydrogen consumed by electromagnet"
```

The results from the solution of the EES code for the calculation of the required hydrogen mass as well as vessel size and volume are given in Figure 36. The size for three permanent magnets as well as levitation forces that are expected from these magnets is given in the results.

Unit Settings: SI K MPa kJ mass deg

A_{em} = 0.001487 [m^2]	A_{pm} = 0.0003325 [m^2]	A_{pmbig} = 0.0009975 [m^2]
B_{pm} = 1.24 [T]	Distance = 480000 [m]	$Duration_{hr}$ = 4 [hr]
$Duration_{min}$ = 240 [min]	$Duration_{sec}$ = 14400 [s]	$Duration_{sec,em}$ = 120 [s]
d_{em} = 0.04351 [m]	d_{pm} = 0.02058 [m]	d_{pmbig} = 0.03564 [m]
E = 1.699E+09 [J]	E_{em} = 1.080E+07 [J]	$E_{specific}$ = 1.199E+08 [J/kg]
F_{em} = 203.4 [N]	F_{pm} = 203.4 [N]	F_{total} = 610.3 [N]
g = 9.81 [m/s^2]	I = 14 [A]	l = 0.55 [m]
L_{em} = 0.015 [m]	L_{tot} = 1.087 [m]	μ_0 = 0.000001257
$m_{container}$ = 32.54 [kg]	m_{H2} = 14.17 [kg]	$m_{H2,em}$ = 0.09005 [kg]
m_{pm} = 20.74 [kg]	m_{sc} = 2.5 [kg]	$m_{support}$ = 13 [kg]
m_{total} = 62.21 [kg]	N = 500 [turns]	P = 10 [MPa]
Power = 118000 [J/s]	$Power_{em}$ = 90000 [W]	r = 0.2647 [m]
$\rho_{container}$ = 4480 [kg/m^3]	ρ_{H2} = 71.26 [kg/m^3]	r_{em} = 0.02175 [m]
r_{pm} = 0.01029 [m]	r_{pmbig} = 0.01782 [m]	SF = 1.088
σ_1 = 661.8 [MPa]	σ_2 = 330.9 [MPa]	σ_3 = 330.9 [MPa]
σ_u = 775 [MPa]	σ_y = 720 [MPa]	Speed = 33.33 [m/s]
t = 0.004 [m]	$V_{container}$ = 0.2061 [m^3]	V_{H2} = 0.1988 [m^3]

Figure 36: Results obtained from solution of EES code given for calculation of required hydrogen mass, storage volume, container size and magnet size.

Appendix C: Superconductor calculations

EES code for the solution of Equation 17 is presented below:

F = 12*(mu_0 * (mu)^2 * t * h * B_1 * (1 + cos(theta)^2)) / (pi * B_2^4) "Force (N) between a magnetic dipole and a superconducting ring"

B_1 = 4*h^2 + t^2 "Constant"

B_2 = -4*h^2 + t^2 "Constant"

t = 0.016 [m] "Superconductor thickness (m)"

{h = 0.0081 [m]} "Distance between SC centre and magnetic dipole"

mu = 0.001 "Magnetic moment"

theta = 0 "Magnetic moment angle"

mu_0 = 4 * pi / 10000000 "Permeability of free space"

gap = h - t/2 "Levitation gap"

g = 9.81 "Gravitational constant"

m = F / g "Levitated mass"

The results of the solution of the code is given in the parametric table below. The levitation forces are given as a function of air gap.

Table 6: Results obtained for the solution of Equation 17 for the magnet and superconductor of this study.

1..11	1 h [m]	2 F [N]	3 m [kg]	4 gap [m]	5 B_1 [m2]	6 B_2 [m2]
Run 1	0.0081	375	38.23	0.0001	0.0005184	-0.00000644
Run 2	0.009	0.0375	0.003823	0.001	0.00058	-0.000068
Run 3	0.01	0.002343	0.0002389	0.002	0.000656	-0.000144
Run 4	0.011	0.0004627	0.00004716	0.003	0.00074	-0.000228
Run 5	0.012	0.0001463	0.00001491	0.004	0.000832	-0.00032
Run 6	0.013	0.00005981	0.000006097	0.005	0.000932	-0.00042
Run 7	0.014	0.00002878	0.000002933	0.006	0.00104	-0.000528
Run 8	0.015	0.00001548	0.000001578	0.007	0.001156	-0.000644
Run 9	0.016	0.000009042	9.217E-07	0.008	0.00128	-0.000768
Run 10	0.017	0.00000562	5.728E-07	0.009	0.001412	-0.0009
Run 11	0.018	0.000003668	3.739E-07	0.01	0.001552	-0.00104

Appendix D: Design drawings

Table 7 lists design drawings and corresponding drawing numbers of each drawing for the design of a cryogenic container for storage of L-H_2, in which an inner vessel is suspended in an outer vessel by means of forces generated between permanent magnets and bulk YBCO superconductors as presented in Chapter 3.

This design also makes use of an electromagnet, for initial suspension while the superconductors make the transition for the normal state to the superconducting state. However a design drawing for the electromagnet and electromagnet rack discussed in Chapter 3.1.1 is not given.

Table 7: A list of design drawings and drawing numbers for a magnetically suspended cryogenic container, which makes use of superconductor thin films suggested as a result of this study.

DRAWING CONTENTS				
ASSEMBLIES	**SUB-ASSEMBLIES**	**PARTS**	**ITEM NO.**	**DRAWING NO.**
HYDROGEN COTAINER CONCEPT				HCC
	INNER VESSEL ASSEMBLY			IV
		INNER VESSEL CYLINDER	1	IV-1
		INNER VESSEL END CAP	2	IV-2
		INNER VESSEL INLET END CAP	3	IV-3
		INNER VESSEL SUPPORT RING	4	IV-4
		INNER VESSEL SUPPORT FRAME BEAM	5	IV-5
		INNER VESSEL HALF RING	6	IV-6
		INNER VESSEL INLET HALF RING	7	IV-7
		SUPERCONDUCTOR	8	-
		SUPERCONDUCTOR CAP	9	IV-8
	INNER VESSEL SUPPORT FRAME			IV-9
	OUTER VESSEL ASSEMBLY			OV
		OUTER VESSEL CYLINDER	10	OV-1
		OUTER VESSEL END CAP	11	OV-2
		OUTER VESSEL INLET END CAP	12	OV-3
		OUTER VESSEL SUPPORT RING	13	OV-4
		OUTER VESSEL SUPPORT FRAME BEAM	14	OV-5
		OUTER VESSEL HALF RING	15	OV-6
		OUTER VESSEL INLET HALF RING	16	OV-7
		PERMANENT MAGNET	17	-
		MAGNET CAP	18	OV-8
	OUTER VESSEL SUPPORT FRAME			OV-9